Properties and Application of Electrochemically Anodized Ta_2O_5 Nanostructures: A Review

Nur Lili Suraya Ngadiman, Rozina Abdul Rani[*]*, Siti Rabizah Makhsin, Muhammad Azmi Ayub*
School of Mechanical Engineering, College of Engineering, Universiti Teknologi MARA, 40450 Shah Alam, Selangor, Malaysia
[*]*rozina7370@uitm.edu.my*

Dharma Aryani
Department of Electrical Engineering, Politeknik Negeri Ujung Pandang, Makassar, South Sulawesi, Indonesia

Ahmad Sabirin Zoolfakar
School of Electrical Engineering, College of Engineering, Universiti Teknologi MARA, 40450 Shah Alam, Selangor, Malaysia

ABSTRACT

Anodization is one of the simplest synthesis methods that can be employed to generate generous nanostructures metal oxide. Knowing the potential of anodized Tantalum Pentoxide (Ta_2O_5) to form the desired nanostructure which is capable to produce outstanding performance, the elements and factors influence properties enhancement were gathered. The effect of parameter variation during anodization such as electrolyte composition, voltage variation, and anodization duration was evaluated to inspect the nanostructure formed. The results generated the differences in properties of nanostructures. Characterization methods such as field emission scanning electron microscopy (FESEM), X-ray diffraction (XRD), Transmission electron microscopy (TEM), Atomic force microscopy (AFM), and X-ray electron spectroscopy (XPS) were used to investigate the structural, electrical, chemical, optical, biological and mechanical properties of anodized Ta_2O_5. The findings show that anodized Ta_2O_5 is reliable to be employed as gas sensor, photocatalysis, pH sensor, biomedical materials and humidity sensor due to its superior properties to produce high sensitivity device and increase the efficiency. In this review, a general overview of anodized Ta_2O_5 is presented which focuses on its fundamental properties, method of synthesis anodized Ta_2O_5, anodization

ISSN 1823-5514, eISSN 2550-164X
Received for review: 2022-07-17
Accepted for publication: 2022-07-31
Published: 2022-11-15

parameter optimization, and recent applications in chemical and biological area, along with a discussion on future research directions relevant to this material. It is hoped that by synthesising nanostructures via anodization, the sensing performance will improve and Ta_2O_5 will be proven as a trustworthy metal oxide material for sensing applications.

Keywords: *Ta_2O_5; Synthesis; Anodization; Nanostructures; Sensors*

Introduction

Nanostructured materials have been broadly studied and enhanced in technologies for the last few years. In particular, transition metal oxide-based aluminium [1], titanium [2], niobium [3], and tungsten [4] were among the materials that have been widely implemented in various electronics applications and advanced catalysts. To synchronize with the nanotechnology industry that rapidly grows these days, these metal oxide materials are commonly studied and fabricated as nanostructures materials and presented in many forms to be employed in sensing devices or as energy storage such as the study of Nb_2O_5 nanochannel as photoanodes [5], W-Ta_2O_5 nanowires in photocatalysis [6], and nanoporous alumina in humidity sensing [7] with nanoscale dimension.

At the nanoscale level, innovative technologies, referred to as nanotechnology, have been compromised, making it feasible to design, produce, characterize, and regulate structures, materials, devices, and systems. Innovative advancements have been made in nanotechnology, especially in the field of nanomaterials, as researchers are discovering structures with varied and distinct attributes that are drastically enhancing numerous aspects of society in the past decades. Nanoscale-materials exist at different dimension structures ranging from zero-dimensional (0D), one-dimensional (1D), two-dimensional (2D) and three-dimensional (3D) nanostructures. Primarily, nanoparticles and clusters are categorized as 0D when all three spatial dimensions are at nanoscales while nanotubes, nanowires, or nanorods are 1D. 2D nanostructures are acknowledged when one of the spatial dimensions are nanoscales such as the structures formed on thin-film or nanosheets. 3D structures are formed when structural elements in 0D, 1D, and 2D materials are in close contact and generate interfaces. Porous nanostructures or compact polycrystals with nanosized grains are known as 3D nanostructures [8].

For many applications, metal oxide nanostructures can be synthesized via different approaches to maximize the surface area of interaction while altering the chemical and physical properties. Synthesis of nanostructure metal oxides can be conducted either in a solid-state, liquid state, or vapour phase deposition such as ball milling [9], hydrothermal [10], sol-gel [11], anodization [12], electrodeposition [13], and physical and chemical vapour deposition [14].

Each synthesis method encounter drawback in their nanostructure's fabrication. For example, hydrothermal method generates a small aspect ratio of 1D nanostructures and requires a few steps of synthesis while sol-gel method is time-consuming with the multistep process. However, these drawbacks in synthesis methods can be encountered through the anodization method which offers the solution based on the weakness of other synthesis methods [15]. Anodization is a form of properties enhancement method that is applicable for metal oxide. It is best known as one of the low-cost synthesis methods [16]. During the process, anodization parameters are varied to investigate various anodization conditions towards metal morphology, structure, and physical and chemical properties. This method is also simpler, able to be manipulated, and structurally tuneable [17]. Development of nanostructures ranging from 0D to 3D can be performed by varying the anodization parameters such as electrolyte composition, anodization time, and anodization voltage. In comparison to sol-gel technique which takes a long time to generate nanostructures on metal oxide, anodization is capable to generate nanostructures with similar dimensions in less duration [15].

Among numerous synthesis methods that allow generating of nanostructures, anodization provides high surface area and ease of repetitive fabrication, which can be considered as an advantage to this method in manufacturing metal oxide nanostructures. Narrowing to the potential of anodized material, outstanding physical and chemical properties can be generated from various anodization parameters which later can provide a favourable surface for the medium of interaction. Copper oxide anodized at certain anodization parameters can exist in the form of nanotubular, nanoporous, nanoneedles, and nanowires, which have the potential to be employed as chemical sensor, corrosion protection, photochemical water splitting, and solar light absorption [15]. There is evidence regarding the use of anodized nanoporous titanium oxide in photocatalytic activity [18]. Meanwhile, nanotubular titanium oxide has the potential to be employed as a biosensor in detecting SARS-CoV-2 as the cause of Corona Virus Disease (COVID-19) pandemic [19] and as bone implant [20]. The nanoporous coating has been fabricated recently from anodized aluminium oxide with the aid of sulphuric acid [1]. The outstanding properties of anodized material have drawn some attention to be used in the electronic industry as well as in biomedical applications.

Enhancement of properties through synthesis method for a particular metal can be a value-added as it improves the function as sensor or battery. Tantalum oxide (Ta_2O_5) is one of the transition-metal oxides that receive significant interest among researchers. In the past recent years, many studies have been conducted concerning Ta_2O_5 performance. Considering the potential of Ta_2O_5 and the anodization method to enhance nanostructures fabrication, the studies related to anodize Ta_2O_5 are gathered. Synthesized Ta_2O_5 has shown excellent results in improvising the properties of metal oxide after

undergoing anodization, which is believed to provide better performance in any practical application or device fabrication for various applications with aided of nanotechnologies. This has influenced the option of Ta_2O_5 over other metal oxides to be implemented in a wide range of applications such as sensors, coating, and biomedical technologies.

In order to explore the potential of anodized Ta_2O_5, its physical and chemical properties are obtained through different characterization methods such as FESEM, TEM, XRD and XPS which can visualize its behaviour. This paper discusses the influence of parameter variation during Ta_2O_5 anodization to alter significant changes in its physical and chemical properties which later improves the Ta_2O_5 performance in sensing application. A brief comparison is discussed in terms of electrolyte composition, voltage variation, anodization duration, and annealing condition as the factors affecting nanostructures. The discussion is projected to further explore the unique properties of anodized Ta_2O_5 obtained through characterization methods. Anodized Ta_2O_5 nanostructures applications in various industries are gathered to observe the effectiveness of anodization compared to other synthesis methods.

Anodization Parameter Optimization

Anodization is regarded as one of the most practical and straightforward procedures in forming extremely porous and ordered nanostructured metal oxide films. To carry out the anodization experiment, an electrode such as a platinum gauze is applied at the cathode and the substrate is attached to the anode. An electrolyte is poured across both electrodes. An anodization voltage is delivered between two electrodes during the synthesis. This causes electrochemical processes to occur on the surface of the substrate, resulting in the formation of a nanostructured metal oxide. The electrolyte composition, applied voltage, and anodization period are all essential parameters that influence the formation of nanostructures and the shape of anodic metal oxide films. Aside from that, metal oxide nanostructures are influenced by the annealing temperature, which occurs after anodization. As-anodized Ta_2O_5 films are mostly amorphous and require post-annealing to be turned into highly crystalline and modify the stoichiometric Ta_2O_5.

Effect of electrolyte composition

Anodization technique is implemented by preparing electrolytes with the adequate composition of the solution before the metal oxide compound can be immersed. From previous studies, electrolyte solution can be composed by combining sulphuric acid (H_2SO_4) and hydrofluoric acid (HF) [21], H_2SO_4, HF and water (H_2O) [22], H_2SO_4, HF, and ammonium fluoride (NH_4F) [23], glycerol and NH_4F [18], H_2SO_4, glycerine, H_2O and NH_4F [24], ethylene glycol, NH_4F, H_2O and H_2SO_4 [25], and NH_4F itself [17]. The concentration

of each element in the electrolyte composition has a significant influence on the growth of nanostructures.

There is a significant reason for adding H_2SO_4 in the electrolyte. It is said that H_2SO_4 is capable of forming nanotubular structure rather than the coral-like which is believed to have better performance in sensing application [24-25]. Increasing the H_2SO_4 saturation in the electrolyte will increase the porosity of nanostructure formation by enhancing the rate of chemical dissolution [26]. Optimization of H_2SO_4 concentration in the glycerol-based electrolyte was conducted by Abu Talib et al. where the concentration of H_2SO_4 was varied by 0%, 0.5%, 0.75%, and 1% [27]. FESEM image indicates voids and tubes of nanostructures best formed with 0.5 %vol of H_2SO_4. Higher concentration is considered to disrupt the formation of nanotubular while no nanotubular can be formed without the content of acid in the electrolyte. In some materials, different types of acid produce different morphology of nanostructures. For example, Mir et al. used three different electrolytes with different types of acids at the same concentration in the anodization of alumina [7]. The pore diameter achieved by anodization of alumina in an electrolyte containing 0.3 M sulphuric acid, oxalic acid, and phosphoric acid was 20 ± 1 nm, 34 ± 1 nm, and 136 ± 4 nm, respectively. This proves that the manipulation in electrolyte elements and concentration is capable to achieve a wide range of nanostructures size.

Fluorine anion can be obtained from sodium fluoride, fluoric acid or ammonium fluoride to be aided in the formation of nanostructures. This statement is supported by Sloppy's calculation which indicates that the dissolution rate of Ta_2O_5 is slow without the presence of fluorine ion in an electrolyte [28]. This is because the dissolution rate of fluorine ion is dependent on its concentration, thus a high concentration of fluorine ion will produce a better etching process towards pore walls, hence, forming nanostructures with a larger diameter [29]. However, as reported by Karuppusamy et al., excessive fluoride ions in the electrolyte may cause no production of nanostructures due to the permanent dissolution of metal oxide [30]. Previous works of literature have reported the presence of NH_4F at different concentrations of NH_4F. The anodization electrolyte is prepared by varying the NH_4F for 0.45 wt%, 1.0 wt%, 1.35 wt% and 3.0 wt% [27]. The findings have shown that 0.45 wt% and 1 wt% of NH_4F content in electrolyte composition is insufficient to produce nanostructures while a sample with 3 wt% indicates that the structure us excessively etched and damaged.

An electrolyte requires organic additives in the formation of nanostructures. The presence of glycerine or ethylene glycol has its competency in increasing the viscosity and conductivity of electrolytes [24]. The presence of glycerine can also change the viscosity of the electrolyte. Given that viscosity is a critical element affecting ion mobility and consequently current density, it is altered by adding varying amounts of glycerol to produce different oxide layer thickness, pore diameter, and

interpore distance. Similarly, the higher the polyethylene glycol (PEG) content, the higher the electrolyte's relative viscosity as it produces lower pore width and thickness of anodic aluminium oxide [31]. As a result, variations in the electrolyte's viscosity are assumed to be a factor affecting ion migration, or perhaps the ionic current through the barrier layer.

In the anodization of Ta_2O_5, electrolyte composition is varied to achieve optimized and most promising nanostructures. To explore the role of water in electrolyte composition, Wei et al. work added an adequate amount of water into glycerol and NH_4F electrolyte. Compared to the aqueous electrolyte, the presence of water during anodization assists in decaying rapid current densities from the initial value [29]. It is strong evidence that the formation of compact oxide is promoted by the presence of water and requires high fluoride concentration to achieve porous layers. Referring to Momeni et al. [23], the researcher anodized Ta_2O_5 into two different types of electrolytes which are made up from the composition of H_2SO_4, HF and ethylene glycol and HF, H_2SO_4, and water respectively. The same anodization voltage of 15 V was applied to both samples. SEM images showed that anodizing Ta_2O_5 for 10 min produces irregular cracks while further elongation in anodization time produces parallel grooves and channels on the film surface. However, the compact film formed without porosity proves that anodization requires the presence of water to produce nanoporous or nanotubes structures.

From the result obtained by manipulating electrolyte composition, it can be said that solution concentration plays an important role in defining the metal properties after anodization. Excellent nanotubular structures can be achieved with an electrolyte composed of ethylene glycol, H_2SO_4, NH_4F, and water with NH_4F as the etching agent for pore formation with the addition of water and H_2SO_4 to increase chemical dissolution rates [27], [32].

Effect of voltage variation

According to Momeni et al.'s [21] research, the morphology of anodized Ta_2O_5 varies depending on the electrolyte composition, voltage applied, pH, and anodizing time. The considerable effect of voltage on the structure of Ta_2O_5 with the change of the voltage applied toward anodizing metal has been discussed in this work. Because the formation of nanostructures is closely related to anodizing voltage, voltage variations are required during anodization to produce an ideal condition in the formation of oxide layer nanostructures.

As anodized, nanotube array films start forming on the surface of tantalum. As higher voltage is applied, the structure and formation of nanotube array films are extended to higher order and become parallel to each other [21]. Nanoporous diameter starts to enlarge as more voltage is applied. Therefore, the formation of the nanostructure oxide layer is highly dependent on anodizing conditions, whether in the form of compact oxide layers, nanoporous, nanotubes, or fishbone structures. High anodizing voltage can directly affect the dissolution degree due to intensive etching which increases

the elongation of nanotube arrays [24]. Meanwhile, a longer nanotube array may result in the detachment of the nanotubes from the tantalum sheet. Therefore, it is critical to manipulate the parameters during the synthesis of tantalum nanostructure to produce a suitable nanotube array.

Momeni et al. [21] prepared two anodizing conditions which were operated at 15 V and 250 V for 120 s and 20 s respectively. After being anodized in the same composition of HF, H_2SO_4, and water as electrolytes and subjected to the corresponding voltage, two distinct samples were tested for corrosion resistance. In this experiment, the formation of nanotube arrays was successfully obtained as the nanotubes order was parallel to each other and perpendicular to the substrate. As higher voltage is applied, oxide layers start to further extend on tantalum result in the formation of nanoporous with a diameter range of 50 nm to 120 nm.

Another anodization of Ta_2O_5 was further investigated by Baluk et. al. [24] regarding the influence of anodizing voltage towards the formation of nanotube array and its adhesion. Few samples were distinguished based on their voltage variation, annealing temperature, and cleaning and drying conditions. Samples were anodized in similar electrolytic and annealing temperature conditions with an anodizing voltage of 10, 15, and 20 V which increased external diameter and length as voltage value increased. However, the adhesion of the nanotube array was weak when 20 V was applied where the nanotubes tended to peel off from Ta foil.

In the formation of nano-dimpled structures by Ma et. al. [12], increasing voltage can increase the diameter of nano-dimpled. Voltage varied between 10 to 70 V which produced nano-dimpled with diameter between 38 to 190 nm. Lee et al. [33] found that a lower voltage of 2 V is only capable to form non-organized pore order with a smaller size. However, the higher voltage applied such as 50 V only forms pores at the outer-most layer. Meanwhile, 20 V applied voltage is capable to form highly ordered pore formation. This is an ideal condition to achieve the desired outcome in K_2HPO_4 and anhydrous glycerol electrolyte setting.

To investigate the effect of voltage potential towards pore diameter and thickness, voltage ranging from 10 to 50 V was applied during anodization using the same electrolyte composition. The pore diameter of the nanoporous structure grew from 13 to 40 nm which can be said as linearly dependent on the voltage applied from 10 to 50 V, at approximately 0.64 nm/V. However, voltage potential higher than 50 V was unable to generate regular pore growth. At this point, the breakdown event took place. Meanwhile, the growth of porous thickness was not linearly dependent on the voltage potential as it increased from about 5.9 μm at 10 V to 15.7 μm at 20 V. There was a sharp decrease following after 20 V. In this case, this pattern is influenced by partial disbonding of layer at this particular voltage potential [29].

Chen et al. [34] reported that at 10 V, the Ta_2O_5 oxide layer appears as nanoporous. After 1 hour of anodization, nanotubes grew with a length of 5.2

μm and a diameter of 40 nm. However, tube formation did not elongate properly. The process continued by increasing voltage potential to 30 V and 40 V. As a result, the top diameter, bottom diameter, and the length of nanotubes at 30 V and 40 V were 57 nm, 72 nm, 20 μm, and 74 nm, 104 nm, 24 μm, respectively [34].

To conclude, a variation of anodization voltage leaves a significant effect on the formation of nanostructures in terms of size, length, and diameter. It is agreed that optimum applied voltage between 20 V to 40 V can stimulate oxide layer growth rates with proper arrangement of pore order [33].

Effect of anodization time

The time of the anodization is one of the parameters that need to be considered to form nanotubular layers. The formation of the parallel channel nanotubular structure indicates higher anodization duration is required compared to the formation of irregular crack structure obtained by shorter duration [23]. As the anodization duration is higher, the formation of nanotube will become obvious. Anodized layer of Ta_2O_5 will dissolve properly to achieve nanotubular structure due to increasing dissolution rate [25]. In most cases, nanotubes grow uniformly when longer duration takes place during anodization.

As reported by Lee et al. [33], at 40 s of anodization time, 10 to 18 nm of pore diameter and 6 to 18 nm of the wall thickness were achieved. At 3 min of anodization time, pore diameter and wall thickness grew until 10–13 nm and 24–28 nm with 20–25 nm of barrier layer obtained. Technically, increasing the anodization time enhances its morphology properties in terms of pore length, pore diameter and thickness.

To further explore the effect of anodization duration towards nanotubes growth, two samples with the same electrolyte composition and a voltage potential at 5 min and 10 min anodization time were compared. The difference in time interval results in different nanotubes diameter, thickness and length. For 5 min of anodization time, the diameter, thickness and length were recorded as 19 nm, 10 nm, 1.27 nm while 21 nm, 10 nm, 3.31 nm were recorded for 10 min of anodization time, respectively. The result obtained shows a further increment especially in terms of diameter and length when the anodization time is prolonged [24].

Hence, it can be said that nanotubes will further grow by lengthening the anodization duration. Anodization process is capable to enhance the morphological properties of Ta_2O_5 including the pore diameter, thickness and nanotube length. This is because, increasing the anodization duration will increase the dissolution rate of metal oxide layer, thus enabling the metal oxide anodized layer to dissolve appropriately during the formation of nanotubes.

Effect of annealing condition

Annealing is a process that involves the application of heat treatment by applying specific heat to metal oxide after the anodization process. As-

anodized samples produce an amorphous structure, and annealing must be carried out to achieve crystalline structure.

From previous studies, Ta_2O_5 underwent annealing in temperature between 150 ºC – 1000 ºC [17], [32], [35], [36]. A lower temperature may result in an amorphous structure while higher temperature might be able to form a crystalline nanostructure [17]. The higher the annealing temperature, the better the nanostructure formation which can also the enhance adhesion of nanotubular [32], [37].

When the Ta film is subjected to anodization, the compact oxide layer may slowly disappear, develop nanoporous and nanotubular structures. Anodization takes place in a constant potential of 15 V for 30 sec to 5 min. As a result, nanotubular formed is well-adhered, with a diameter formation at 40 nm and tube length at 1 μm. After annealing takes place, diameter and tube length increase to 45 nm and 2 μm, respectively.

Knowing the potential of Ta_2O_5 in forming nanostructure at a different phase, a study was carried out to transform the amorphous nanoporous into a hexagonal phase. As-anodized Ta_2O_5 generates an amorphous structure on its oxide layer. XRD pattern in Figure 1 shows that after annealing at 290 ºC, the structure transforms into a hexagonal structure which decreases the pore size ranging from 23 to 49 nm. Minagar et al. [38] also found that the hydrophilic property and the surface energy of the hexagonal nanoporous layers of Ta_2O_5 increased after the annealing process.

Most of the previous studies required high annealing temperatures above 300 ºC to be applied on Ta_2O_5 to transform the amorphous phase into crystalline. This condition might be due to its high melting point that requires high thermal treatment to achieve the crystalline phase. Depending on the observation, the result indicates that the influence of thermal treatment plays an important role in the nanostructures phase to enhance crystallinity and alter Ta_2O_5 physiochemical properties [39].

As the potential of anodization has been acknowledged, this method was implemented to other metal oxides as well such as TiO, Al_2O_3, ZnO, and Nb_2O_5. Table 1 summarizes the effect of the anodization parameter on the morphology of nanostructures. The variation of anodization parameters in terms of electrolyte composition, anodization voltage, anodization duration, and annealing condition alters the dimension of nanotubes length, thickness, and pore diameter. The trend of synthesizing metal oxides using anodization has been increasing in the recent 5 years which proves that this is a reliable method to create novel nanostructures. However, some gap has been determined between the studies. Most of the nanostructures are fabricated using current anodization parameters generating nanoporous, nanodimpled, and nanotubular structures. There is no evidence reported on other kinds of nanostructures such as nanochannels, nanorods, and nanowires composed of anodized Ta_2O_5.

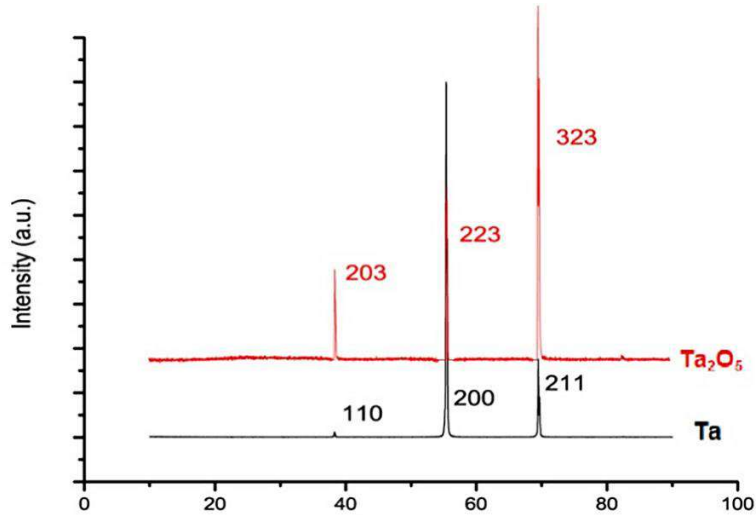

Figure 1: Comparison of XRD pattern between tantalum foil and Ta_2O_5 after annealing which shows the transformation from amorphous nanoporous into hexagonal phase. Permission open access from [38]

Anodization Mechanism in the Formation of Nanotubular Ta_2O_5

Formation of nanotubes from nanoporous structures

Anodization is an electrochemical method that is used to construct the naturally existing oxide layer on metal surfaces like Nb, Al, Ti, Ta, Cu, V, and Zr. It is often carried out in a two-electrode electrochemical cell, with the metal serving as the anode and platinum serving as the cathode. Oxygen ions generated at the electrolyte/anode interface move under the action of the electrical field, migrate within the metal attached to the anode and form an oxide surface layer when a potential difference between the electrodes is applied [40]. It is possible to manipulate electrochemical parameters, such as anodization duration and voltage, as well as electrolyte concentration, temperature, and pH, to change the characteristics of oxide layers and create novel surface morphologies like nanotubes, nanochannel, nanowires, and nanodimples on transition metal.

Table 1: Summary on nanotubes length, thickness and pore diameter of Ta_2O_5 formation according to electrolyte composition, variation, anodization duration and annealing condition

Morphology	Substrate	Electrolyte composition	Anodization voltage	Anodization time	Dimension
Nanotubes [18]	TiO film	Glycerol, H_2O, NH_4F	60 V	6 h	D: 90-100 nm T: 20-25 nm
Nanoporous [93]	Al_2O_3 film	Oxalic acid	20 V, 40 V, 50 V	3 h, 1 h, 40 min	D: 31.8, 53.1, 71.0 nm
Nanoporous [94]	Fe_2O_3 film	EG, NH4F, H2O	40 V	1 h	D: 59 ± 2 nm
Nanotubes [2]	Ti_6^4 plates	EG, NH_4F, H_2O	60 V	1 h	D: 120 nm
Nanoporous [40]	Ta Tilm	H_2SO_4, HF	30 V	5 – 20 min	D: 25 – 65 nm
Nanoporous [17]	Ta_2O_5 thin film	NH_4F, EG	15 V	2 h	D: 8–10 nm T: 3 nm
Nanoporous [78]	Ta_2O_5 film	Millipore water, HF, H_2SO_4	-	10 min	T: 45±2 nm;
Nanoparticles [95]	Zn film	HCO_4	20 V	1 h	particles sizes: 10 – 20 nm
Nanotubes [29]	Ta film	Glycerol, NH_4F,	20 V	3 h	D: 17 nm
Nanotubes [29]	Ta film	Glycerol, NH_4F, H_2O (1 – 10 ml)	20 V	3 h	T: 39 nm – 138 nm
Nanotubes [23]	Ta film	H_2SO_4, HF, EG	15 V	10 – 20 min	T: 2 µm D: 55 nm
Coral-like [48]	Ta film	EG, H_2O, H_3PO_4, NH_4F	20 V	1 h	30 nm to 50 nm.
Nanotubes [24]	Ta film	H_2SO_4, glycerine,	15 V	5 – 10 min	L: 1.27 – 3.31 µm T: 10 nm
Nanotubes [21]	Ta film	H_2O, NH_4F Hf, H_2SO_4, H_2O	15 V – 250 V	20 s – 120 s	D: 41 – 42 nm D: 50 nm - 120 nm
Nanoporous [67]	Ta film	K_2HPO_4, glycerol	-	40 s – 180 s	T: 6 nm – 25 nm D:10 nm- 28 nm

Nanotubes [29]	Ta film	Glycerol, NH_4F	10 V – 50 V	3 h	T: 5.9 µm 15.7 µm
Nanotubes [38]	Ta film	HF, H_2SO_4, H_2O	15 V- 250 V	-	D: 50 nm -120 nm
Nanotubes converted to nanodimpled [56]	Ta film	NH_4F, H_2O, diethylene glycol, H_2SO_4	7 V – 70 V	-	L: 2−9 nm D: 25−60 nm

Ta_2O_5 nanotubular growth mechanism occurs in four stages that begin with the formation of the oxide layer by tantalum hydrolysis, following by pore deepening, initial nanotubular formation until nanotubular structures are perfectly formed, as summarized in Figure 2 [27].

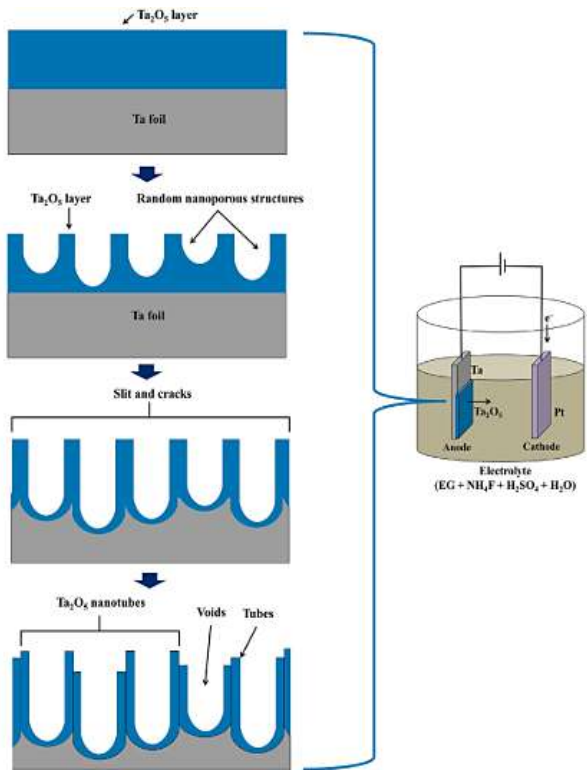

Figure 2: Illustration of Ta_2O_5 nanotubular growth mechanism during anodization. Permission open access from [27]

At the first stage, the oxide layer starts to form and due to its low electrical conductivity and electric field-enhanced dissolution of the oxide layer, this oxide layer significantly reduces the anodization current resulting in the formation of first pores. Development of the tantalum oxide layer and acid-induced dissolution processes leads to the development of nanostructured surface features in the anodization of tantalum. The nanotubular structure requires the presence of F− ions, which cause chemical etching to generate porous and self-aligned Ta_2O_5 ordered architectures [41]. In contrast to other acids, sulfuric acid (H_2SO_4) is characterized by high thermodynamic stability, and it plays a key role in promoting the uniform development of nanotubes. F− may be extracted from sodium fluoride or fluoric acid, which are among the most common chemical components. The $[TaF_7]^{2-}$ anions are an important component in the development of nanotubes. Ionic species such as F- and O^{2-} migrates from the electrolyte to the metal-metal oxide interface while tantalum ions flow in the opposite direction under the applied potential to form Ta_2O_5 nanostructures. While optimizing anodization parameters to fabricate nanoporous surface features, it is important to acknowledge that higher etching rates are better achieved using a more concentrated electrolyte, resulting in the formation of nanotubular features. Meanwhile, lower etching rates are found when using a less concentrated electrolyte, resulting in a compact oxide layer. For the nanopores to form, it requires the electrolyte to be concentrated enough to promote the right concentration of F− ions to partially dissolve the readily formed oxide layer. Hence, it is necessary to increase the electrolyte concentration so that the oxide layer dissolves in a way that would then form the nanopores on the surface.

Next, the dissolution of Ta_2O_5 begins, and pores develop following the separation of one pore from another, resulting in the establishment of distinct tubes that are vertically aligned with the substrate. The applied electric field promotes the production of field-assisted transport of Ta5+ and O2- and the dissociation of O^{2-} from H_2O for which the chemical interaction leads to Ta_2O_5 being formed. Following the increment in anodization duration, fluoride ions are found deeper into the tantalum matrix and interact with tantalum, resulting in a higher anodization average pore size [40].

The formation mechanism of nanopores during anodization may be described by the I–t curve in Figure 3 [40]. The occurrence of anodization produces a barrier layer on the tantalum surface that causes the current to raise in a short period. Following the development of the compact Ta_2O_5 layer in region a, a substantial reduction in current is noticed, since the current is unable to pass through the layer. Due to the dissolving reaction of fluoride ions, tiny pits appear on tantalum oxide in region b and transform into porous structures. Fluoride ions dissolve in the barrier oxide that causes the current going through the electrochemical cell to rise. The maximum current is attained at the end of region c. A steady drop in current occurs in region d as the current diffusion rate is limited due to the oxide formation and dissolution processes in the pores.

The pH value of electrolyte solution after anodization is slightly lower compared to before anodization takes place. This is because if the anodizing is kept on for a longer period, it could promote acid dissolution, which will then cause the adjoining pores to merge [42].

The length of NTs is highly dependent on the voltages, temperatures, and periods applied during anodization. To obtain a high etch rate and improve the dissolving rate of oxide layers, it is advisable to use a higher voltage during the anodic oxidation. However, a too high voltage supply may cause the nanotubes to be extracted from a tantalum sheet if they are longer than the length at which they can be pulled off. Thus, it can be assumed that applying the appropriate condition of anodic oxidation to a tantalum sheet results in a synthesizing of Ta_2O_5 nanotubes that adhere well to a substrate [24].

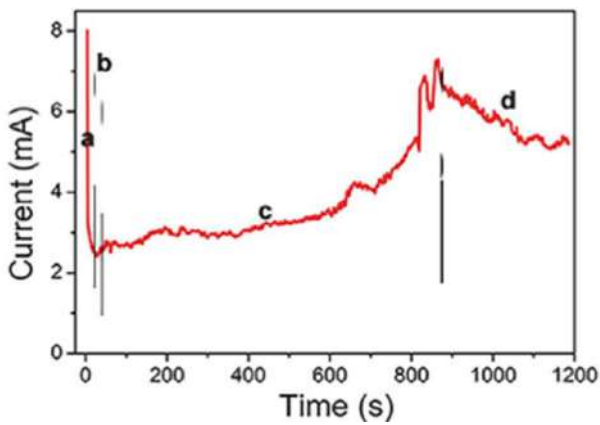

Figure 3: Current-time graph obtained during anodization of tantalum to reveal the current behaviour during the formation of nanoporous tantalum oxide layers up to 20 min anodization time. Reprinted from [40] 2020 with permission from Wiley Periodicals, Inc.

Chemical reaction during anodization

When neutral Ta is anodized in acidic aqueous electrolytes, an associated electric field is effectively capable of inducing the oxidation of neutral Ta with H_2O to facilitate the anodic transition of neutral Ta into Ta_2O_5 [43]. The half-cell reactions at anode and cathode and net reactions of the reduction process occur as in Equations (1), (2), and (3), respectively:

$$Ta \rightarrow Ta^{5+} + 5e^- \quad (1)$$

$$2H_2O + 2e^- \rightarrow 2OH^- + H_2 \quad (2)$$

$$2Ta + 10H_2O \rightarrow 2Ta^{5+} + 10OH^- + 5H_2 \quad (3)$$

An oxide layer is built up on the metal by Ta hydrolysis at the electrolyte/metal interface, as described in Equation (4). Oxide barriers generated in anodic oxide can be fairly dense. The electrolyte may either dissolve or partially dissolve the anodic oxide. To produce a steady state of oxide formation and dissolution, an anodization parameter should be used to control the rate of oxide production and dissolution where porous metal oxide will grow under these conditions [44].

$$2Ta + 5H_2O \rightarrow Ta_2O_5 + 10H^+ + 10e^- \quad (4)$$

As seen in Equation (4), H^+ rises during hydrolysis, and F ions then travel to the H^+ sites to establish electroneutrality and fight for the O_2 sites in the oxide. To generate a tantalum oxide passivation layer on Ta foil, tantalum hydroxide is produced in tantalum hydrolysis. At a steady voltage, the oxide layer is created in the electrolyte. Acidification of the electrolyte could result in the development of large amounts of gaseous compounds because of water hydrolysis as shown in Equation (5).

$$2H_2O \rightarrow O_2 + 4H^+ + 4e^- \quad (5)$$

A regular arrangement of nanopores occurs, ranging from a cylinder form to the more generalized round, with a diameter of fewer than 100 nm. Equation (6) depicts the conversion of Ta to Ta^5 through oxidation.

$$2Ta + 5H_2O \rightarrow 2Ta^{5+} + 10H^+ + 10e^- \quad (6)$$

Cation vacancies located at the metal /oxide contact allow for the reaction in Equation (6), which enables the Ta^{5+} to hop to the accessible vacancies. Nanopores form on the oxide surface while this condition is occurring. The concentration of F- in the pores grows fast as H+ ions are produced at the bottom of the hole where the Ta comes out of the metal and dissolves in the solution. Increasing in F- exposure leads to the breaking down of porous walls until the neighbouring pores completely vanish. The size of pores also increases as the surface integration occurs [27]. At the same time, the increased electric field-assisted dissolution further enhances the process, therefore developing the voids. By stimulating the electric field, increased dissolution helped by the electric field is used to develop the pore, therefore developing the voids. The applied electric field promotes polarisation and metal oxide disintegration, as a result of which the Ta-O bond loses strength. This Ta is releasing ions which form acid in the pore bottom and affect pH profile developing in the pore development direction. Dissolution occurs

towards the bottom of the pore rather than at the top, resulting in a longer nanotubular.

Lastly, TaF_7^{2-} is formed from Ta_2O_5 by the local dissolution of H+, F–, and O_2 to a critical level. Chemical dissolution influences the pore area grows as the Ta_2O_5 dissolving rate increases in fluoride-containing fluids, as stated in Equation (7). Negatively charged cation vacancies are formed in Ta after it has dissolved, and they migrate to the metal/oxide interface because of a potential gradient that forms across the oxide.

$$Ta_2O_5 + 14F^- + 10H \rightarrow 2[TaF_7]^{2-} + 5H_2O \quad (7)$$

The oxide layer that forms when anodization occurs in an acidic solution is rather compact. Due to these limitations, self-organizing nanoporous oxide layers of these metals cannot be produced. Fluoride anions are necessary for the creation of self-organizing nanostructured coatings to solve this problem. Fluoride is unique in that it creates water-soluble metal-fluoride complexes, preventing the growth of metal-oxide layer build-up at the tube bottom. F− ions, which have a greater migration rate across the oxide lattice, and have a lower ionic concentration than O^{2-} ions. This is what initiates the nanostructured coating growth since it induces the creation of a fluoride-rich layer at the metal-oxide contact. Figure 4 describes the process of the anodizing method of nanotube arrays development mechanisms of electrochemical anodization and the development of anodization electrolyte composition by generation [45].

Due to rapid oxide dissolution, the first generation of nanotube synthesis faced several challenges. Hence, HF was swapped with KF or NaF to improve the pH and increase the nanotube length in the second generation. With the third generation of synthesis, the length of the NTs was increased in non-aqueous electrolytes, such as ethylene glycol (EG), dimethyl sulfoxide (DMSO), formamide (FA), dimethylformamide (DMF), and N-methylformamide (NMF) with HF, NH_4F or KF mixed in. Currently, the fourth generation of nanotube synthesis has been found, which employs non-fluoride electrolytes and used in the anodizing of titanium [45].

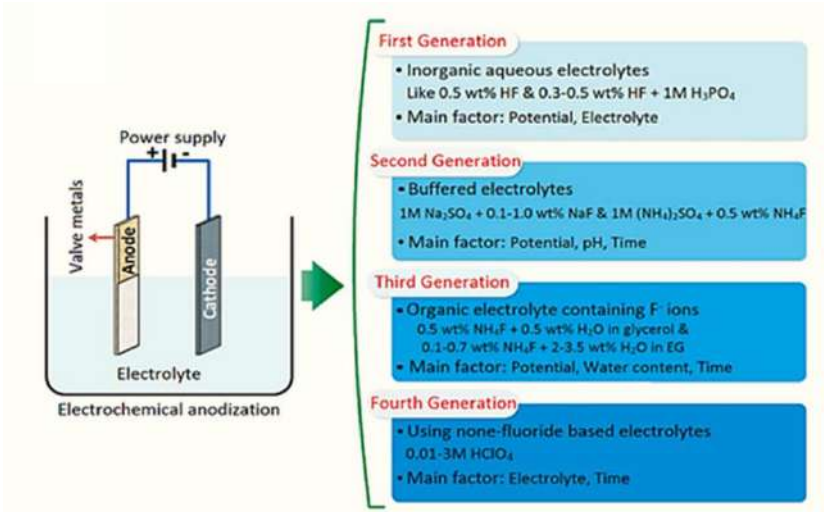

Figure 4: Different generation of TiO_2 nanotubular fabricated sing anodization synthesis method. Reprinted from [45] Copyright 2020 with permission from Elsevier

Anodization Parameter Optimization Properties of Ta_2O_5

Structural properties

Nanostructures of Ta_2O_5 are present in various structural features and shapes such as nanoporous, nanodimpled, nanotubes, and coral-like. The measurement of Ta_2O_5 morphology can be accessed through SEM, FESEM, or AFM. These analysis tools visualize the morphology and topography of nanostructures such as pore diameter, thickness of oxide layer, pore length, pore wall, surface roughness, and cross-sectional thickness.

Synthesis method such as electrospinning was used to synthesize Ta_2O_5 nanofibers Ta_2O_5 with average length and diameter of 40 nm and 12 nm, respectively [46]. As in the case of Ta_2O_5 nanospheres formation with ultrathin hollow spherical shell in size ±5nm, a facile template method has formed Co_3O_4/ Ta_2O_5 hollow nanospheres with the diameter ranging from 100 nm to 300 nm [47]. There was evidence from the one-step hydrothermal method to construct Ta_2O_5 nanorods and W Ta_2O_5 nanowires. The length and diameter of these nanowires were reported to be 0.7-1.2 μm and less than 30 nm, respectively [6].

Similar to other synthesis methods, different nanostructures of Ta_2O_5 can be obtained through anodization. As discussed in the previous section, electrolyte composition is one of the anodization parameters that contribute to

a different nanostructures formation to alter the morphologies of Ta_2O_5. For instance, the use of phosphoric acid (H_3PO_4) is said capable to form coral-like of Ta_2O_5 [14], [25]. In a study conducted by Yu et. al. [48], anodization electrolyte was composed of a combination of Ethylene Glycol, water, H_3PO_4, and NH4F that resulted in the distribution of uniform nano-scaled pores on Ta_2O_5 film in an assembled morphology of coral-like structure. Nanoporous Ta_2O_5 with pore diameter ranging from 5 to 35 nm and oxide layer thickness of about 400 nm was anodized in an electrolyte containing HF or H_2SO_4. The formation of pores was randomly located with narrow size distribution. The distribution of pores, size and thickness can be manipulated by varying the electrolyte concentration, anodization time and voltage applied during the anodization reaction [14]. Nanotubes can be grown from the increment in voltage potential or duration during anodization [34]. Replacement of HF to NH_4F is a strong factor for the growth of nanotubular from nanoporous structures [45]. Minagar et al. [38] obtained the top view, bottom view, and cross-sectional view of nanotubular Ta_2O_5 with the diameter ranging from 35 to 65 nm and nanostructure thickness of 1.17 ± 0.05 μm. Wen et al. [49] reported that the morphology of Ta_2O_5 nanotubes produced with different current densities and anodizing times differs, which is primarily reflected in the nanotubes' length and diameter. The length of the nanotubes increases as the anodizing current density and time increase. The results show that Ta_2O_5 nanotubes of 18 μm length can be grown in less than 2 minutes at a current density of 125 mA cm^{-2}. Under constant current anodizing conditions in the H_2SO_4–HF electrolyte system, Ta_2O_5 nanotubes grow at a faster rate than under constant voltage anodizing conditions. These findings could pave the way for large-scale production of Ta_2O_5 nanotubes in the future. Figure 5 displays coral-like, nanoporous, and nanotubes structures as the formation of the potential nanostructures during anodization synthesis of Ta_2O_5.

Initially, the nanoporous structure started to form compact oxide layer once anodization began. Prolong anodization transformed the nanoporous structure to nanotubular. Other than structure formation, anodization time gives a different effect on Ta_2O_5 nanotubular surface roughness that is measurable through AFM which displays surface topography of the oxide film based on colour intensity to indicate roughness. Anodizing at 0.5 h produced surface roughness of 38.90 nm while anodizing at 1.0 h and 1.5 h produced surface roughness of 63.93 nm and 95.94 nm, respectively. It is said that higher surface roughness is capable to adsorb a higher number of oxygen molecules which results in rapid photoconductivity activities and enhancement in responsivity [25].

Another evidence has reported on topography properties of anodized Ta_2O_5 film treated with and without n-octadecyltrichlorosilane (OTS) which has been analysed through AFM. Result acquired has indicated that Ta_2O_5 film without OTS has 2.5 nm surface roughness while Ta_2O_5 film with OTS has 1.3 nm surface roughness. The anodized oxide layer is grown in a homogenous,

uniform manner and appears to be smoother that facilitates the low threshold voltage organic thin-film transistors with low surface roughness [50]. The literature has shown that anodization is capable to generate a wide range of Ta_2O_5 surface roughness between 1 to 100 nm that can be utilized in the various application according to its compatibility.

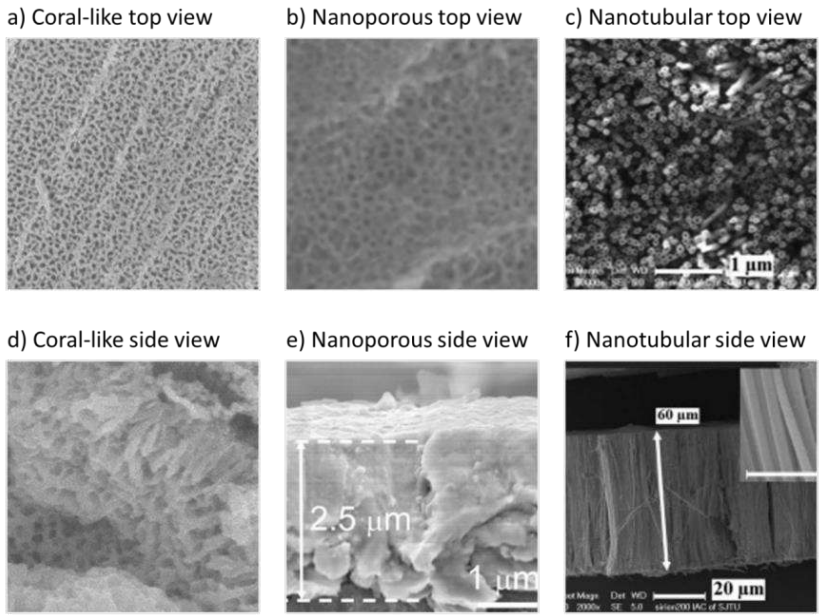

Figure 5: FESEM and SEM images of top view and side view Ta_2O_5 with three different types of nanostructures grown from different electrolyte composition by comparing (a) coral-like top view [48], (b) nanoporous top view [17], (c) nanotubular top view [34], (d) coral-like side view [48], (e) nanoporous side view [17] and (f) nanotubular top view [34]. (a and d) Permission open access from [48]. (b and e) Reprinted from [17], Copyright 2018, with permission from Elsevier. (c and f) Reprinted from [34] Copyright 2017, with permission from Elsevier

From this evidence, we can see the importance to manipulate anodization parameters to create a novel structure of metal oxide with distinct dimensions favourable for respective applications. This has justified that anodization is a good alternative for the synthesis of nanostructures into a different form such as nanotubes, nanoporous, nanodimpled and coral-like as the parameters are feasible to be manipulated. Based on previous studies, this simple method has successfully generated pore dimension at the nanoscale that can be employed accordingly to different applications.

Chemical properties

After anodizing in a sulphuric acid-containing electrolyte, the nanostructure of Ta_2O_5 contains impurity sulphur and excess oxygen. The presence of these impurities might probably cause the structure to become more stable and enhance its stability properties [51]. Once anodization takes place, the formation of a compact oxide layer is presented on the tantalum surface. Tantalum ions (Ta^{5+}) released from tantalum metal become soluble once they reach the oxide layer and electrolyte, thus forming $[Ta_7]^{2-}$. Hence, a pore is formed between the oxide layer interface and electrolyte. The pore formation further develops during the process as anodization assists to trap the necessary ions. Growth rates of anodized nanostructures such as nanoporous and nanotubes are influenced by the rate of diffusion of fluorine ions and metal complex solubility [38].

In comparison to other anodized transition metals such as titanium, tantalum has a higher rate of oxidization. Formation of tantalum nanoporous mechanism has a close relation with $[Ta_7]^{2-}$ molecular dimension, Ta_2O_5 formation kinetics, and formation enthalpy. Low electrode potential is required to oxidize tantalum compared to titanium. In terms of forming enthalpy, tantalum releases more calories than titanium. Hence, it is highly agreed that the rate of oxidization of tantalum and formation of an oxide layer on the substrate surface is faster than titanium where its standard formation enthalpies are −492.790 and −228.360 gram calories per mole, respectively [38].

Compared to anodized Nb_2O_5, Ta_2O_5 possesses higher lithium storage capacity due to its Ta-O bond that is less robust than Nb_2O_5 in Lithium batteries application [5]. The amorphous structure of Ta_2O_5 develops a narrower bandgap and conveys desirable electrochemical activity. Furthermore, oxidation of tantalum occurs at different oxidation states such as +5 (Ta_2O_5) and +4 (TaO_2). Oxidation of +5 (Ta_2O_5) can be said as the most stable state. Passivation layer formed on the tantalum surface when permitted to air exposure results in unparalleled corrosion resistance. This is why tantalum can strongly resist chemical attacks from strong acid hydrochloric acid or nitric acid. Hence, strong etching agents such as hydrofluoric acid, fuming sulfuric acid and potassium hydroxide are capable to etch Ta_2O_5 [52].

XPS analysis visualizes the elemental and chemical bonding state as the characterization of Ta_2O_5 [32]. This method can be used to prove the formation of an oxide layer after anodization which is indicated by the photoelectron intensity peak of the anodized region binding energy for both tantalum and oxygen atoms [49], [52]. The measurement was done by measuring atomic concentrations for Ta and O atoms [33]. Corresponding to the Ta 4f7/2 and Ta 4f5/2 orbitals, synthesis of Ta_2O_5 via one-step heating has obtained Ta 4f element approximately located at two peaks centered at 26.5 eV and 28.4 eV using XPS. Meanwhile, O element was located at 530.4 eV and 532.3 eV corresponding to 1s orbital [54]. Figure 6a shows the XPS spectra for elements in Ta_2O_5. A facile template method used to synthesize Co_3O_4/ Ta_2O_5

heterostructure hollow nanospheres indicated the two strong peaks at 25.7 and 27.5 eV with the gap of 1.8 eV of Ta 4f spectrum, which significantly belonged to Ta2O5 with a valence of +5. Oxygen species in the Ta_2O_5 were observed around 530 eV in the O 1s spectra [47]. For nonporous tantalum, Ta 4f7/2 and Ta 4f5/2 peaks appeared at 21.6 and 23.5 eV, respectively, which were characteristic peaks of metallic tantalum [40].

In another literature for the synthesis of Ta_2O_5 conducted via anodization, it was found that Ta 4f element was identified at 26.3 and 28.2 eV while O element was located at 530.6 and 532.6 eV which supported the appearance of Ta and O component at approximately similar peaks [17]. Subsequently, peak binding energies for Ta 4f5/2 at 26.3 eV and 26.5 eV were observed in nanoporous Ta_2O_5 fabricated by Fialho et. al. [42]. In the deconvolution of Ta4f, the corresponding doublet was revealed with Ta 4f5/2 at 26.48 eV and Ta 4f3/2 at 28.38 eV, both of which were related to the Ta5+ state from Ta_2O_5, which had a spin orbital splitting of 1.9 eV. The spectrum revealed by O 1s showed an interesting deconvoluted feature with a peak at 530.55 eV, which correlated with Ta_2O_5 being the main contributor. Two other O 1 peaks occurred at 531.69 and 532.81 eV, supporting the existence of hydroxyl and carboxyl groups. Anodized Ta_2O_5 developed by one-step anodization in a fluoride (F^-) containing electrolyte illustrated a single peak at 684.68 eV of F 1s spectrum, which can be associated with the fluoride ions adsorbed on Ta_2O_5 aided by an electric field and dissolved into the anodic layer [55]. Other studies exhibited similar peaks of Ta 4f and O 1s spectra for anodized Ta_2O_5 nanostructures located at similar peaks which indicated that strong chemical attributes can be obtained through anodization [49], [52], [55], [56].

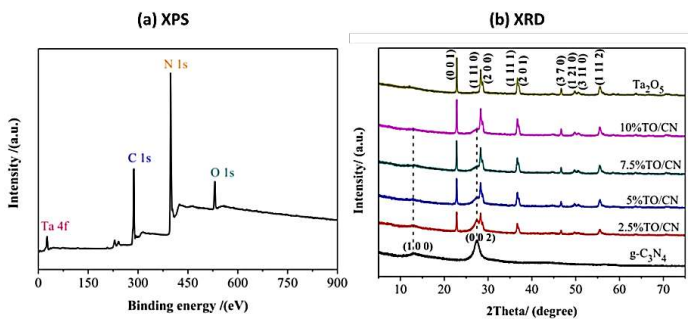

Figure 6: (a) XPS spectra indicates chemical composition of 7.5%TO/CN heterojunction photocatalyst and (b) XRD result showing diffraction peaks of pure Ta_2O_5, 2.5% Ta_2O_5/g-C_3N_4 heterojunctions (TO/CN), 5% TO/CN, 7.5% TO/CN, 10% TO/CN and bare g-C_3N_4 identified to represent different crystalline structure. Reprinted from ref [54] Copyright 2017, with permission from Elsevier

Crystal structure

Similar to other metal oxides, Ta_2O_5 has polymorphic transformation of about 10-15 which has been reported until this date and can be identified by XRD [37], [57]. As-anodized structures are primarily amorphous and require post-heat treatment to transform into a crystalline structure. β-Ta_2O_5 phase can exist at low temperature while phase transition to α-Ta_2O_5 requires a high temperature above 1000 ºC [41], [58]. Crystal structures of metal oxides have commonly existed in the form of triclinic, monoclinic, orthorhombic, tetragonal, trigonal, hexagonal, and cubic. One of the impressive Ta_2O_5 crystal attributes formed via anodization is its potential to generate wide ranges of crystal structures using Ta foil and Ta_2O_5 powder as substrate. Monoclinic crystal structure is commonly found at low-temperature post-heat treatment [6] while hexagonal and orthorhombic can be achieved at a high temperature of above 550 ºC [35], [53], [59], [60], [61]. For most cases, anodization possesses a slightly similar trend where annealing at 400 ºC produces cubic structure while increasing the temperature up to 750 ºC produces tetragonal structure and following temperature increment of above 800 ºC can generate orthorhombic crystal structure as shown in Table 2 [42], [50], [54], [62].

Regardless of the anodization voltage, Ta_2O_5 nanotube arrays grow in an amorphous phase until the sample is being annealed [34], [38]. Annealing at high temperatures will result in the transformation of amorphous oxide into the crystalline phase. All diffraction peaks are identified, and the largest five peaks are determined to correspond to degrees of crystallinity, which indicates the crystallization behaviour of the sample [51]. Initially, annealing at 1058 K is found to be in the amorphous state. However, after annealing in 1128 K, the crystalline structure of orthorhombic β- Ta_2O_5 is able to form diffraction peaks identified at 22.9°, 28.4°, 36.8°, 46.7°, and 55.5° [51]. There is also evidence that annealing in 700 ºC is able to form hexagonal phase with peaks appearing at 23°, 28.5°, 36.5°, 50.5°, and 55.5°. Figure 6b visualizes the Ta_2O_5 peak for orthorhombic structure. By increasing annealing temperature to 800 ºC, the crystalline structure transforms from hexagonal to orthorhombic with diffraction peaks at 50.5° being split into 50° and 51° [64].

Another characterization method that can be used to characterize the crystal phase of Ta_2O_5 is TEM imaging. Variation of chemical phases including measurement of nanoparticles size, size distribution, grain size, and morphology with clear interfaces can be obtained. Total sample thickness, period, and sub-layer thicknesses are also possible to be measured through TEM [65]. There is a slight difference in image formation using TEM and SEM which can be seen in Figure 7 since the TEM images are created using transmitted electrons whereby the electrons are passed through the sample to create an image. The microstructure layer of Ta_2O_5 is characterized as amorphous with a gap value of 2000 Å (< 100 Å) [66]. Different chemical interfaces can be observed through TEM analysis where the interplanar distance of pure Ta is 2.33 Å; thus, it identifies crystal plane 111 of α-Ta for

all crystallinity [65]. TEM is able to provide porosity of selected area diffraction pattern in which as-anodized Ta_2O_5 porous structure can obtain porosity of 26% which indicates its amorphous nanostructures [33]. Crystal plane of 020 with fringe interspace of 5.1 Å is identified as orthorhombic [16].

Table 2: Crystal structure according to their post-heat treatment temperature based on substrate and synthesis method

Substrate	Synthesis method	Crystal structure	Post-heat treatment temperature (°C)	Ref
Ta_2O_5 and S-doped Ta_2O_5 nanocomposites	Sol-gel method	Orthorhombic	700	[61]
Ta_2O_5 powder	Facile one-step heating	Orthorhombic	550	[54]
$Tacl_5$ powder	Ultrasound-assisted	Orthorhombic	800	[60]
Ta_2O_5 doped tungsten	Hydrothermal	Monoclinic	200	[6]
Ta_2O_5 powder	Hydrothermal	Hexagonal	550	[62]
Ta_2O_5 deposited on silicon	Ion beam sputtering deposition	Hexagonal	800	[35]
Ta_2O_5 deposited on silicon	Ion beam sputtering deposition	Orthorhombic	1000	[35]
Ta_2O_5	Template-assisted	Orthorhombic	700	[96]
Ta foil	Anodization	Orthorhombic	800	[51]
Ta foil	Anodization	Hexagonal	290	[38]
Ta foil	Anodization	Cubic	400	[42] [55]
Ta foil	Anodization	Tetragonal	750	[42] [55]
Ta_2O_5 powder	Anodization	Cubic	400	[63]
Ta_2O_5 powder	Anodization	Orthorhombic	800	[63]

Biological properties

Ta_2O_5 possesses outstanding thermal and chemical stability and its biocompatible properties are promising. Thus, its capability to be used as a biosensor and biomaterial is undoubted. Another interesting property exhibited by Ta_2O_5 is low toxicity due to a high oxidation state. Ta_2O_5 is highly inert and

biocompatible which makes it widely used in biomedical applications as biomaterial as well as resistance to acid corrosion [11], [14]. Until today, there has been no evidence regarding its cytotoxicity that may harm osteogenic cells and mesenchymal stem cells. In biomedical application, a natural protective coating is produced by forming oxide layers on the surface of tantalum during anodization which relatively provides extra protection for cells. Although the amorphous state of nanoporous is unable to generate nanotubular, this state will form linkages or platforms for allowing it to combine with certain drug during the drug loading process [64]. Ta_2O_5 has also been widely used as implant material based on its biocompatible properties [32], [66], [67].

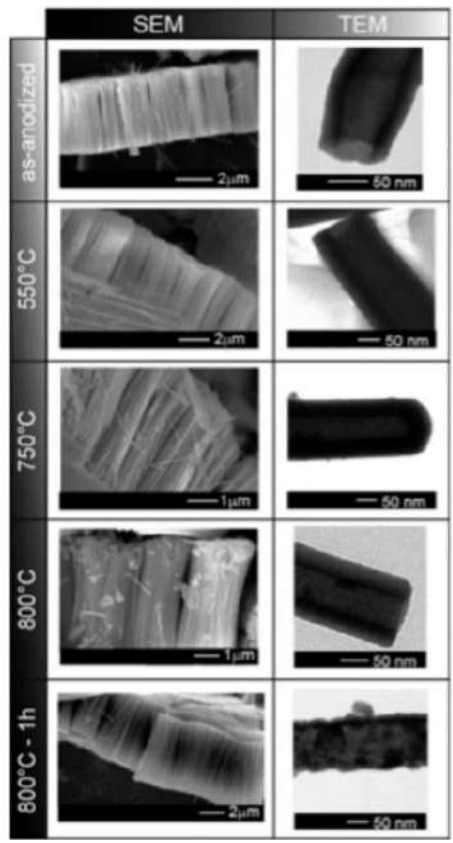

Figure 7: Comparison on image formation of Ta_2O_5 nanostructures, as anodized and annealing at different temperatures obtained using SEM and TEM. Reprinted with permission from [39] Copyright 2012 American Chemical Society

Compared to Nb_2O_5, TiO_2, and ZrO_2, Ta_2O_5 has the highest bioactivity of biocompatible nanoporous and nanotubular oxide metals in simulated body fluid at 37 °C measured after 3 weeks. This performance is indicated by the atomic ratio of calcium to phosphate due to absorption of Ca^{2+} ions onto the hydrolysed nanoporous and nanotubular oxide surface following the adsorption of existing phosphate groups to the positively charged surface inside the simulated body fluid; thus, forming calcium phosphate. Deposition of hydroxyapatite (HA) is observed on as-formed and annealed Ta_2O_5 film as shown in Figure 8.

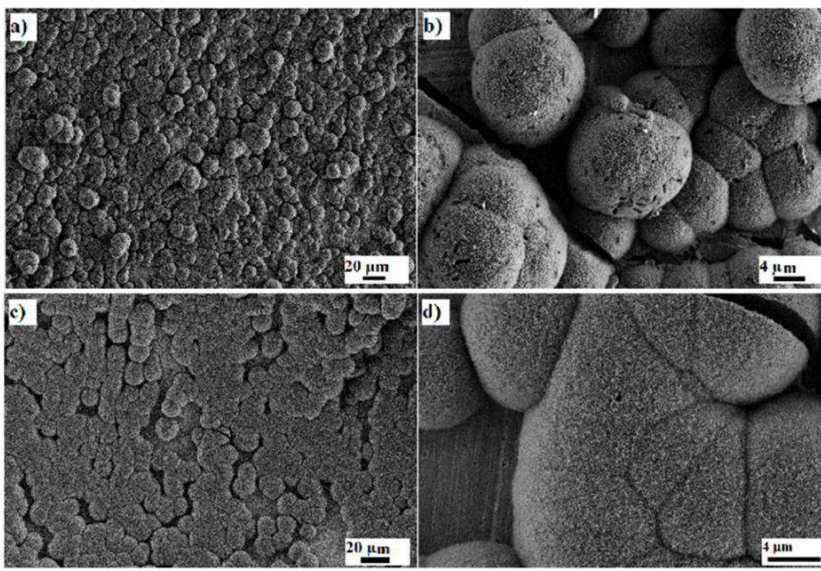

Figure 8: SEM images of (a) low magnification and (b) high magnification Ta_2O_5 deposited with Hydroxyapatite (HA) on (c) formed and (d) annealed film. Permission open access from [38]

Referring to Figure 9, the performance of Ta_2O_5 is indicated by the presence of a mixture of calcium and phosphate in compositions HA of bone composition [38]. It was found that biological properties possessed by anodized nanoporous tantalum oxide promoted fibroblast adhesion and proliferation, as well as the growth of fibroblasts on the anodized surfaces. Strong cellular adhesion on nanoporous tantalum with the higher surface interaction was recorded by tantalum nanoporous with 25 nm pore size [40]. Anodization of tantalum alters its surface topography and enhances the hydrophilicity of the porous tantalum [12]. On the other hand, nanodimpled Ta_2O_5 produced via anodization exhibits higher hydrophobic properties than

pure tantalum. Nanodimpled with a diameter of 90 nm has the highest cellular activity of adhesion towards mouse cranial anterior bone cells. Hence, the properties of anodized Ta_2O_5 can be manipulated and fabricated according to its favourable condition for application.

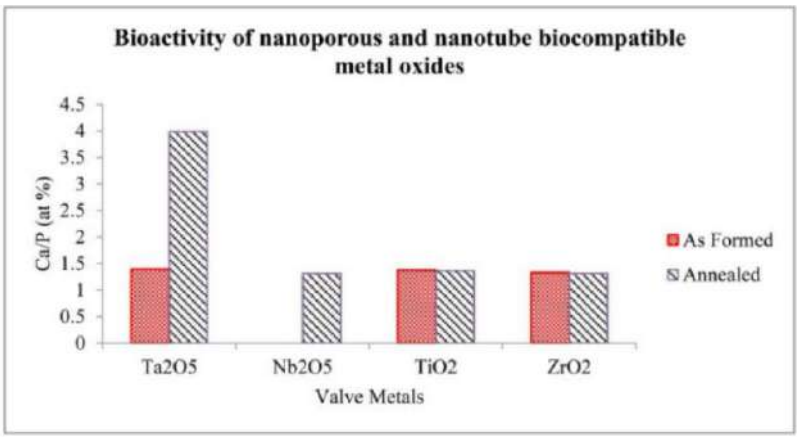

Figure 9: Atomic ratio of calcium to phosphate indicates by hydroxyapatite (HA) deposition to measure bioactivity performance of metal oxide after 3 weeks in modified simulated body fluid (m-SBF) between as-formed and annealed Ta_2O_5, Nb_2O_5, TiO_2 and ZrO_2. Permission open access from [38]

Optical properties

The reason why Ta_2O_5 is one of the best candidates for the optic-based sensor is that it exhibits high refractive index material which might enhance the sensitivity of the sensor [21], [57], [68], [69]. The presence of defects level and oxygen vacancy on its surface has aided in productive interaction by quickly adsorbing analyte molecules in the sensing surface [71].

To demonstrate the optical energy band gap of Ta_2O_5 nanoparticles prepared by ultrasound-assisted synthesis, UV–VIS diffused reflectance spectroscopy was used to investigate its optical properties. The study projected the bandgap for Ta_2O_5 nanoparticles as 3.12 eV which was slightly lower than the bulk Ta_2O_5 (3.8 eV) [60]. The green light emission of this Ta_2O_5 nanoparticles appears to be at its most intense level at a wavelength of 535 nm with a particle size of 20 nm. Since these nanoparticles have excellent luminescent properties, they can be used in optical devices and high-quality monochromatic lasers. Electronic band structure of β-Ta_2O_5, δ-Ta_2O_5 and orthorhombic with lattice parameter a = 7.9 Å, and b = c = 3.75 Å were applied [72]. Calculated band gap produced 2.45 eV, 2.92 eV and 3.7 eV respectively. As Ta_2O_5 can exist in many crystals form in which each structure suits the certain condition of application, the existing of various Ta_2O_5 form produces

different band gap which allows optical properties control according to its functional suitability. Ta_2O_5 has a minimum absorption at ultraviolet light, which is known as the adsorption edge around 320 nm. This occurs due to the intrinsic band gap of Ta_2O_5 being around 3.9 eV [60], [72].

As the amount of Ta doped on the TiO_2 layer increases, the overall photocurrent density decreases. The gradual enhancement of the optical band gap in combination with decreasing photocurrent is consistent with the Ta concentration (from 3.31 to 3.44 eV). In this application, an ultrathin Ta-doped TiO_2 layer was applied to exhibit photoelectrochemical activity. This layer responded with photoelectrochemical currents of about 10–100 mA/cm^2 upon exposure to UV light (wavelength 320–380 nm; intensity 2.5 mW/cm^2) [74].

According to Nickel et. al., the composite refractive index of metal oxide can be enhanced either by increasing anodization voltage or with a certain mixture of anodization electrolyte composition to increase the pore diameters [75]. The addition of chemical additives in anodization might also agitate to increase the refractive index by decreasing the dissolution rate. From the study, it was found that anodization of aluminium-tantalum thin film in 0.4 M phosphoric acid at 4 V was able to generate a refractive index of 1.258 while additional of 0.1 M oxalic acid and 0.4 M oxalic acid into the electrolyte mixture is capable to increase the refractive index to 1.319 and 1.359 respectively. Chemical addictive such as oxalic acid reduces chemical etching; hence, decreases the pore size which reduces the air content in the thin film. As a result, the refractive index of the porous aluminium oxide layer increases due to a decrease in air content within the oxide layer [75]. Modification of optical properties is possible through anodization as synthesizing the nanostructure will alter the electronic band structure.

Mechanical properties

Porous tantalum is highly advantageous due to its mechanical properties especially in biomedical applications compared to solid tantalum. It was found that the elastic modulus of porous tantalum was 1.3–10 GPa which was lower than solid tantalum and titanium alloy which were 186 GPa and 106–115 GPa respectively. Meanwhile, the elastic modulus of porous tantalum was nearly close to cortical (12–18 GPa) and cancellous (0.1–0.5 GPa) bone tissue. The stress shielding effect can be reduced as it possesses a low elastic modulus [14].

The porosity of porous tantalum was 75%–80% while the porosity of other porous materials was 75%. Higher porosity value regulates tissue permeability and enhances the exchange of nutrient inside scaffold which potentially leads to tissue growth [14]. The porous structure exerted by Ta_2O_5 has approximately similar mechanical properties of natural bone.

Compression tests carried out using a servo-hydraulic MTS (axial/torsion materials test system) machine found that Young's modulus of laser-processed Ta samples can be varied in the range of 2–20 GPa [68]. In

comparison to the actual human trabecular bone, porous tantalum fabricated through chemical vapour infiltration and deposition and powder metallurgy technique is capable to create approximate properties as shown in Figure 10.

Meanwhile, Ta_2O_5 was seen to improve in corrosion behaviour after annealing took place as reported by Sarraf et al. [32], where it was analysed by using nanoindentation device result in maximum hardness of ~ 7.5 GPa and elastic modulus of ~ 160 GPa. Compared to its bare substrate, the modification for corrosion resistance was almost 50% and 29% higher. In addition, the enhancement of Ta_2O_5 durability properties can be done through the manipulation anodization duration [24].

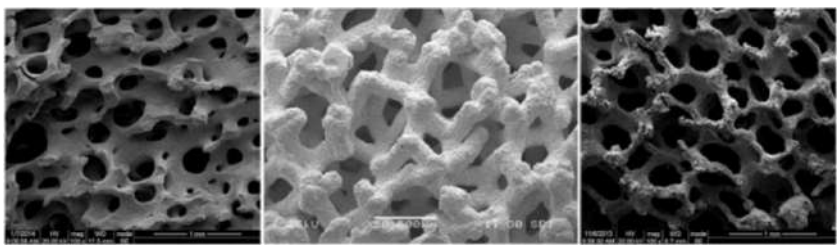

Figure 10: Image of Scanning electron micrograph (SEM) displaying actual human trabecular bone (left), porous tantalum fabricated through chemical vapour infiltration and deposition (CVI/CVP) (middle) and powder metallurgy (PM) (right) technique. Reprinted from [14] Copyright 2015, with permission from Elsevier

Application of anodized Ta_2O_5

In this section, the use of anodized Ta_2O_5 in chemical and biological applications is presented. Based on the literature conducted, Ta_2O_5 use is relatively small; thus, many material possessions can be explored and various novelties can be obtained with a more comprehensive and detailed study. In addition, the application of Ta_2O_5 synthesized using other methods is also discussed and compared to its performance.

Gas sensors

Ta_2O_5 has been found to exhibit assorted functions in sensing applications due to its extensive sensing properties. In relation to metal oxide gas sensors, it has been demonstrated that the use of nanoheterostructures can enhance their performance as the doping mechanism has improved the oxygen vacancy available on the structure [76]. While doping increases the concentration of oxygen vacancies, this has been shown to enhance chemisorbed oxygen concentrations.

A study focused on a capacitive hydrogen sensor made of an ultra-permeable Ta_2O_5 dielectric film on a SiC substrate tested with the range of

hydrogen concentrations from 0 to 2000 ppm in room temperature to 500°C. After 60 seconds of exposure to 2000 ppm hydrogen gas at 500°C, the capacitance increased from 5.0 to 6.5 nF. The proposed hydrogen sensor using a thin Ta_2O_5 dielectric film showed good sensitivity and adaptability at high temperatures. Pd-capped tantalum is excellent optical hydrogen sensing material [77]. The sample exhibits a much-defined optical response to hydrogen, with excellent resolution. There is no hysteresis observed and the optical response of the materials to hydrogen is stable over time.

Another test study conducted by Imbault et al. investigated the efficiency of Ta_2O_5 nanoporous as a permeable oxide membrane for gas sensing [78]. The fabrication of the sensor includes the placement of the Ta_2O_5 membrane on the top layer of platinum electrodes through the implementation of the Lift-Off-Float-On technique. The response of Ta_2O_5 towards carbon monoxide, hydrogen, ethanol, and ammonia was recorded and its efficiency was analysed in an active sampling of diluted analytes. A sensing membrane of 1 cm in diameter was capable to sample the airflow of a few hundred milliliters per second to obtain the presence of analyte molecules. It is reported that the use of Ta_2O_5 to construct a nanoporous membrane for gas sensing devices is due to its properties that exert high redox chemical activity at elevated temperatures above 400 °C. The chemical and thermal stability properties of Ta_2O_5 has made it known as superior materials for sensing properties which lead to high selectivity and sensitivity.

A study was carried out by Zhang et al. [47], where the implementation of Co_3O_4- Ta_2O_5 heterostructure took place in an ethanol gas sensor. It has been seen that this formation possessed an outstanding sensitivity, selectivity, and stability performance which exhibited ethanol gas sensing properties enhancement compared to ZnO-Co_3O_4 and Co_3-SnO_2 heterostructure. This is because Ta_2O_5 nanostructures with ultrathin hollow spherical shells hinder the aggregation of Co_3O_4 nanoparticles while acting as the supporting model. It is claimed to possess more active sites and a higher surface area for adsorption of gas molecules. In this case, aside from Ta_2O_5 selectivity properties, more surface-adsorbed oxygen species are available to react with the target gas, which leads to an enhanced response. In addition, an increase in oxygen chemisorption is also mentioned as being caused by a larger surface area.

Photocatalytic activity

Ta_2O_5 nanostructures exhibit quite promising properties to provide wide surface area and magnificent charge transport and separation. Due to its optical properties which exert a high refractive index, Ta_2O_5 has become a good candidate for photocatalytic application [57], [69]. Several studies have been reported regarding the implementation of Ta_2O_5 related to photocatalytic activity.

Nanostructures of Ta_2O_5 have desired properties in the photoelectrochemical water splitting application as reported by Su et al. [16].

The hydrogen production photocatalytic performance of the heterojunctions created from the Ta_2O_5/g-C_3N_4 is massively better than the pristine g-C_3N_4. The photocatalytic hydrogen evolution efficiency of the 7.5% TO/CN heterojunction was about 4.2 times higher than that of pure g-C_3N_4. Furthermore, the 7.5% TO/CN sample demonstrated excellent photochemical stability after 20 hours of photocatalytic testing [54]. Besides, TiO_2- Ta_2O_5 (2:1 ratio) photo-catalyst mixed oxide prepared by Patil et al. [62] through the hydrothermal method and calcinated at 600 °C had the highest percent degradation of 99.48% in 60 min. A study reported on β-Ta_2O_5 nanodimple arrays had an electronic band gap of 4.5 eV and a bulk plasmon resonance at 21.4 eV formed via anodization was enhanced by 40% of its plasmonic photocatalysis function after being embedded with gold nanoparticles which proved that surface modification can be employed on anodic Ta_2O_5 to increase the efficiency [56]. Table 3 summarizes the performance of Ta_2O_5 in photocatalytic activity based on anodization, hydrothermal, solvothermal, and sol-gel synthesis methods.

pH sensing

The issues raised from pH sensor fabrication are the complexity of the method, expensive materials, require the reference, other than sensor accuracy and response time which affect the reliability of the sensor. Many studies have been conducted to investigate the use of Ta_2O_5 as a material in pH sensors. However, there is still a gap in the literature of the fabrication of pH sensors from anodized Ta_2O_5. The mechanism of the pH sensor works is conducted by representing the concentration of hydrogen ions in a solution and portraying it in a significant value known as pH [9]. Ta_2O_5 has often being selected as pH sensor fabrication due to its pH-sensitive properties towards H^+ ions [79]. There were many studies on the fabrication of pH sensors using Ta_2O_5 either using it alone or combined with other oxides for this purpose.

Ta_2O_5 based electrolyte-ion sensitive membrane-oxide-semiconductor (EIOS) pH sensor for the acid environment was made up of thermally grown SiO_2 with Ta deposited using radio-frequency (RF) sputtering. This sensor was tested in the 1 to 10 pH range and obtained a Nernstian value of 56.19 mV/pH [80]. Using a similar method of RF sputtering, the Ta_2O_5 membrane was employed to IrO_2 to enhance the H+ response towards the pH sensor [81]. It maintains the Nernstian value of −59.447 to −59.504 mV/pH for pH ranging between 2 to 13. The previous performance of Ta_2O_5 showed high sensitivity and low drift which has drawn significant attention regarding the implementation of Ta_2O_5 in this application [82].

Table 3: Performance of Ta_2O_5 in photocatalytic activity based on synthesis method of Tantalum

Synthesis method	Materials	Photocatalytic mechanism	Degradation / evolution rate	Photocurrent	Efficiency	Ref
Anodization	Ta plate coated with Al layer, nanoimprinted with Si and mask anodization to form Ta_2O_5 nanorod array	Water splitting under UV irradiation	-	1.5 ma/cm2 at 1 V versus RHE	0.69% at 2.9 ma cm^{-2}	[58]
	Ta film with thickness of 0.1mm converted to Ta_3N_5 nanotube arrays	Illuminated photoelectrodes with AM 1.5G-simulated sunlight at 100 mw cm-2	10 mv/s	5.9 ma/cm2 at 1.23 VRHE 12.9 ma/cm2 at 1.59 VRHE	-	[16]
	Ta foil with thickness of 1 mm	Degradation of the MB under UV light in 3 different electrolytes containing ethylene glycol (Sample A), glycerol (Sample	Sample C exhibits the highest photocatalytic activity for MB degradation due to the ability of	-	-	[23]

		B) and HF + H_2SO_4 + H_2O (Sample C)	electrolyte to generate nanotubes on Ta_2O film			
	Ta foil with thickness of 0.25 mm loaded with NiO	Photocatalytic reactions for hydrogen production	7.7 ± 0.3 mmol/h/g	-	-	[22]
Hydrothermal	TiO_2-Ta_2O_5	Degradation of methylene blue (MB) under UV irradiation.				[62]
Solvothermal	$Tacl_5$ powder turns into Ta_2O_5 powder self-doped with Ta^{4+}	Evaluated by degradation rate of Rhodamine B dye as organic pollutant model	-	-	3.6 % at 447 nm	[70]
Sol-gel	Ta Ethoxide liquid turns into Ta_2O_5 white crystal	Evaluated by degradation rate of MB dye	-	1.3 μa/cm2	-	[97]

Performance enhancement of pH sensor requires high sensitivity, fast response, and low power consumption, where the morphology of porous and nanostructured thick film has a high surface-to-volume ratio due to a large number of adsorption [79]. These properties can increase sensor efficiency. A collective study of pH sensor fabrication based on Ta_2O_5 with good Nernstian value indicates favourable medium of interaction with H^+ ion provided by Ta_2O_5 structure. The performance of anodized Ta_2O_5 in pH sensing is yet unexplored. However, evidence from the fabrication of pH sensors from anodized amorphous TiO nanotubular generates great output [83]. TiO_2 nanotubes length fabricated at 33 nm to 800 nm by anodizing between 10 to 90 minutes generated response time of less than 30 s and 54.5 mV/pH Nernst response. Hence, the anodization method has the potential to enhance Ta_2O_5 performance towards H^+ detection.

In pH sensing application, important parameters such as Nernstian response, response time, hysteresis width, drift, offset, and isothermal current need to be highlighted in the resulting yield. These parameters are used to measure the efficiency of the metal oxide pH sensor. Meanwhile, the synthesis method gives a significant influence on electron transfer and ion exchange performance as the outcomes.

When two electrodes are immersed in a test solution, the potential difference between the electrodes is generated. The value is expressed by the Nernst equation where the potential difference is proportional to the pH of the solution. Nernstian potential dependence on solution pH is determined by H^+ /OH^- ions. The time required for a sensor to reach more than 90% of its open circuit potential value in equilibrium is defined by the response time. Obtaining different output voltage for a pH electrode measured in the same buffer solution is where the Hysteresis phenomenon occurs. Hence, it is determined by measuring the potential change of a solution after dropping 0.1M HCl or KOH into it [79]. Besides, by calculating the initial and the final voltage difference at a particular pH, drift potential can be determined [84].

The use of Ta_2O_5 as material in pH sensor and its performance are recorded in Table 4 by gathering Nernstian response, response time, hysteresis width, and drift for each pH sensor fabrication [78], [79], [80], [81], [83], [84]. An example of pH sensor fabrication is illustrated in Figure 11a by implementing Ta_2O_5 as a sensing electrode. Figure 11b visualizes the sensing performance of RuO_2-Ta_2O_5 (70:30%) thick film [79].

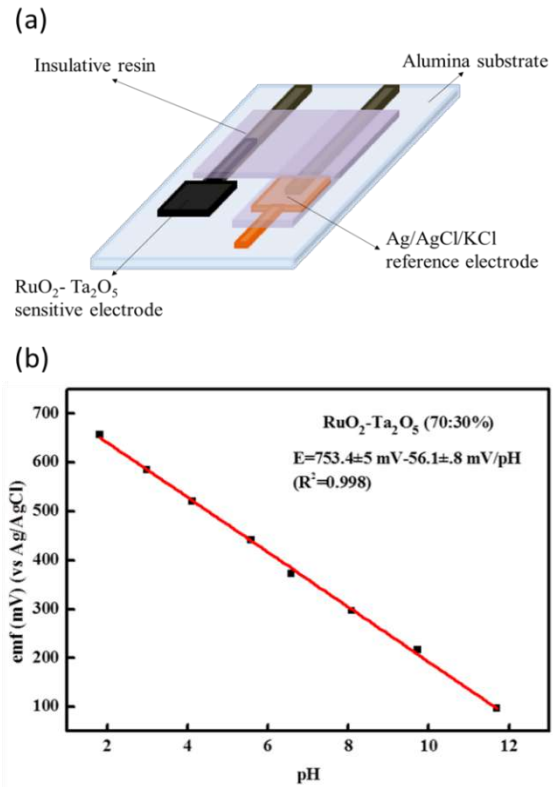

Figure 11. (a) The schematic diagram of pH sensor fabrication using Ta_2O_5 as electrode and (b) RuO_2-Ta_2O_5 (70:30%) thick film sensor potential performance. Reprinted from [79] Copyright 2016, with permission from Elsevier

Table 4: Synthesis method and sensing performance of Ta_2O_5 based pH sensors material

Materials	Synthesis Method	Nernstian response (mV/pH)	Response time (s)	Hysteresis Width	Drift	Ref
Ta_2O_5	Atomic Layer Deposition	53.6 for 39 cycles 55.3 for 200 cycles	-	-	0.017 mV/s	[84]
Ta_2O_5	Thermal oxidation	56.19	-	~5 mV for pH loop 7-4-1-4-7-		[80]
IrO_2-Ta_2O_5 films on	Wet-oxidation	59.447 to 59.504	-	-	-	[81]
Ta_2O_5	Ball milling	45.92	-	-	-	[82]
RuO_2- Ta_2O_5	Ball milling	56	>8 s in acidic solutions, >15s in basic solutions	±3 mV for pH loop 2-4-6-4-2, ±8 mV for pH loop 7-9-11-9-7	-	[79]
WASFET with Ta_2O_5 as the top gate oxide layer	Oxidation	58.8 ± 0.2	-	-	< 0.02 mV/h	[85]
Anodized Ta_2O_5 nanotubular	Anodization	31.616 and 24.591	20 s and 90 s	-		[98]

Biomedical materials

For the past five years, many kinds of research have been conducted to validate the efficiency of Ta_2O_5 as a sensing layer in biomedical applications. Either being used alone or doped with other materials, Ta_2O_5 is still capable to provide an outstanding outcome during the performance testing. Looking from the perspective of Ta_2O_5 potential as biomedical materials, regardless of the synthesis method, Ta_2O_5 can perform in many various aspects. The fiber-optic sensor has been constructed with a surface plasmon resonance optical scaffold by varying the composition of Ta_2O_5 and Graphene as thin layers with Ta_2O_5 thickness that varies from 2 nm to 12 nm [71]. Sensing probes are prepared with Ta_2O_5 layer, Graphene layer, and both Ta_2O_5-Graphene layers. The combination of Ta_2O_5-Graphene layers resulted in a higher magnitude of field intensity by probes with the Ta_2O_5 layer. This outcome proves that Ta_2O_5 has the ability to enhance fiber-optic sensing performance due to higher sensitivity. Besides, the formation of a biosensor such as a xanthine sensor can be constructed by synthesizing Ta_2O_5 nanostructures through the electrospinning technique [46]. Optimization of a sensing probe made up of xanthine oxide entrapped with Ta_2O_5 nanofibers coating produces a linear operating range of 0 to 3 µM which increases the sensing performance.

Many factors can contribute to its ability to generate reliable outcomes. Besides Ta_2O_5 itself, the anodization method has gained much trust as one of the excellent synthesis methods to enhance Ta_2O_5 properties. Anodization is able to form nanostructures that have the ability to improve in the application by varying its parameter such as electrolyte, voltage applied time interval, and annealing. Other than the evidence of anodized Ti used as coating and bone-implant [20], anodized Ta_2O_5 nanostructures possess outstanding nanomechanical properties to be employed as a coating. Sarraf et al. [32], demonstrated excellent performance of Ta_2O_5 nanotubes with 45 nm inner diameter having the highest corrosion protection of 99% efficiency.

Fabrication of Ta_2O_5 nanoporous through various techniques is capable of imitating the biological properties of human structures which makes it relevant to be implemented in various biomedical applications. The comparison of Ta_2O_5 nanoporous through chemical vapour infiltration and deposition (CVI/CVP) (middle) with powder metallurgy (PM) has physically and mechanically resembled actual human trabecular bone as shown in Figure 9 [14]. Nano-dimpled Ta_2O_5 fabricated via anodization adheres to mouse cranial anterior osteocytes (MC-3T3-E1) cell lines to obtain fluorescence microscopic observation and physicochemical characteristics. Variation in anodization voltage potential increases nano-dimpled structure formation. In contrast to pure Tantalum, increment in pore sizes that can grow between 40 to 90 nm is able to promote the adhesion, proliferation, and differentiation of MC-3T3-E1 cells [12]. This proves that anodization can be used as a synthesis method to enhance Ta_2O_5 performance and obtain the optimum dimension for functional use.

Humidity detection

Humidity detection happens when metal oxide surfaces come into contact with water vapour in the atmosphere or a pure gas [85], [86], [87]. Water adsorption is facilitated in this case by the simultaneous action of the metal oxide's active sites and water molecules. Also, the large surface area of adsorption allows humidity detection to be performed more effectively [89]. In the production of humidity sensors, Ta_2O_5 serves as a sensing layer material. Active sites for interaction media are established on thin-film oxide layers. The surface area available for interaction is influenced by voltage bias and impurities doping. The concentration of water molecules is associated with the moisture level in an atmosphere. In sensor detection, water molecules interact with the oxide layer by adsorption and desorption.

Grotthuss's mechanism principle is widely utilized for most current humidity sensors. In this mechanism, hydrogen bonding serves as the means of proton transfer from one water molecule to its adjacent molecules, resulting in the proton hopping condition [90]-[91]. Surface water at low relative humidity has a high charge carrier density, which attracts hydroxide ions on the surface [91]. The chemisorbed layer is formed due to the adsorption of the hydroxyl group to the Ta_2O_5 oxide layer. An increase in RH increases the water molecules' ability to dissociate, which then releases more hydroxyl groups. Two hydroxyl groups of a water molecule interact with two nearby water molecules by hydrogen bonding and the physisorption (first layer) is formed. When RH concentration increases, the second layer of physisorption is formed on the Ta_2O_5 surface with more water molecules ionized to form H_3O^+. While the proton transfer has occurred rapidly and H_3O^+ can separate into H_2O and H^+, more water adsorption can begin with a further rise in the pH level [10].

For tantalum-based humidity sensor fabricated to this date, Potassium carbonate (K_2Co_3, 99%), niobium pentoxide (Nb_2O_5, 99.5%), tantalum pentoxide (Ta_2O_5, 99%), and manganese dioxide (MnO_2, 99%) was synthesized through a conventional solid-state reaction route and then used to fabricate a tantalum-based resistive humidity sensor, which exhibited a maximum sensitivity of 4600 tested with relative humidity between 15% to 95% at constant 5V bias voltage [86]. The role of tantalum in humidity sensing was once again investigated using the fabrication of tantalum-based interdigital electrodes coated with rGO-SnO_2. By varying 11% to 95% relative humidity over 30 days, this sensor exhibited good sensitivity, rapid response, and long-term stability with the response and recovery times of 10 s and 60 s [92].

More evidence was collected from the nanostructures-based humidity sensor. The sensitivity of the nanoporous alumina anodized in oxalic acid solution has a pore diameter of 34 ± 1 nm and porosity 10 ± 0.5 % that reaches up to 0.21 (pF/%RH). Pore diameter and interpore distance increase the anodic alumina porosity, allowing more water molecules to penetrate and providing more surface area for detection. Thus, the anodic alumina humidity sensor

features improved performance because of its tiny pore structure and uniform nanopore distribution [7]. 40% to 90% relative humidity (RH) was put in contact with a metal-semiconductor-metal humidity sensor made from anodized nanoporous Nb_2O_5 with platinum electrodes, and different bias voltages were applied. The relative sensitivity of 4-µm-thick Nb_2O_5 nanoporous Nb_2O_5 structure under a voltage bias of 5 V was determined to be 216.5, resulting in the nanoporous Nb_2O_5 presenting the highest sensitivity. This high surface area to volume ratio in the sensors provides highly effective interactions and bindings between active sites and water molecules [3]. This allows the potential of anodized Ta_2O_5 to be further explored as Ta_2O_5 has a good record for H^+ interaction while considering the nanostructure potential to enhance the water molecules interaction in humidity sensors [99].

Conclusions

In conclusion, the advantage of anodization synthesis method is widely known as it is capable to alter properties according to application requirements by varying its parameter. Ta_2O_5 exhibits outstanding properties as well as thermal and chemical stability which makes it among the best candidate to be implemented in various applications. Anodization of Ta_2O_5 requires a strong etching agent to increase the dissolution rate during pore formation due to its ability to withstand chemical attacks. Hence, this is why Ta_2O_5 is commonly chosen as coating materials aside from being implemented in sensing applications. Nanotubes generation can be enhanced in terms of its length by increasing anodization voltage potential and undergoing thermal treatment afterward. Annealing often takes place after anodization to crystalline as-anodized amorphous state which makes Ta_2O_5 possess extensive properties before fabrication of sensor can be done.

This review justifies the potential of anodization to modify Ta_2O_5 nanostructures and enhance its properties as this method can generate a wide range of nanostructure dimensions that are favourable as medium of interaction. Since Ta_2O_5 has its selectivity to interact with certain molecules, anodization prepares the Ta_2O_5 nanostructures to improve the adhesion and facilitate the sensing process. Various applications have been found by employing Ta_2O_5 either to use it alone or dope with other materials through different synthesis methods such as solvothermal, sol-gel, and ball milling. Future studies will carry out to use Ta_2O_5 as a sensing application as well by performing anodization as a synthesis method to recognize the potential of this method towards Tantalum film. Performance comparison can be made in terms of selectivity, sensitivity, and efficiency for single use of Ta_2O_5 and dope with other materials. By synthesizing the nanostructures through anodization, it is believed that this method can enhance the sensing performance and prove Ta_2O_5 as a reliable metal oxide material for sensing application.

Acknowledgement

This work is supported by the Ministry of Education Malaysia (MOE) under the Fundamental Research Grant Scheme (FRGS) FRGS/1/2019/TK07/UITM/02/7 (Project Code: 600-IRMI/FRGS 5/3 (389/2019)).

References

[1] F. A. Bruera, G. R. Kramer, M. L. Vera, and A. E. Ares, "Low-cost nanostructured coating of anodic aluminium oxide synthesized in sulphuric acid as electrolyte," *Coatings*, vol. 11, no. 3, pp. 1–16, 2021, doi: 10.3390/coatings11030309.

[2] M. Sarraf, N. L. Sukiman, A. R. Bushroa, et al, "In vitro bioactivity and corrosion resistance enhancement of Ti-6Al-4V by highly ordered TiO_2 nanotube arrays," *Journal of the Australian Ceramic Society*, vol. 55, pp. 187 - 200, 2019.

[3] R. A. Rani, A. Sabirin, M. F. Mohamad, A. S. Ismail, and M. H. Mamat, "High Surface Area to Volume Ratio 3D Nanoporous Nb_2O_5 for Enhanced Humidity Sensing," *Journal of Electronic Materials*, vol. 48, pp. 3805–3815, 2019, doi: 10.1007/s11664-019-07126-5.

[4] M. Jamal, K. M. Razee, S. Han, J. Islam, and I. Ak, "Development of Tungsten Oxide Nanoparticle Modified Carbon Fibre Cloth as Flexible pH Sensor," *Scientific Reports*, vol. 9, no. 4659, pp. 1–9, 2019, doi: 10.1038/s41598-019-41331-w.

[5] R. A. Rani, A. S. Zoolfakar, J. Z. Ou, R. A. Kadir, H. Nili, K. Latham, S. Sriram, M. Bhaskaran, S. Zhuiykov, R. B. Kaner, K. Kalantar-zadeh, "Reduced impurity-driven defect states in anodized nanoporous Nb_2O_5: The possibility of improving performance of photoanodes," *Chemical Communications*, vol. 49, no. 56, pp. 6349-6351, 2013, doi: 10.1039/c3cc42998a.

[6] M. M. Momeni, M. Mirhosseini, and M. Chavoshi, "Growth and characterization of Ta_2O_5 nanorod and WTa_2O_5 nanowire films on the tantalum substrates by a facile one-step hydrothermal method," *Ceramics International*, vol. 42, no. 7, pp. 9133–9138, 2016, doi: 10.1016/j.ceramint.2016.03.002.

[7] M. A. Mir, M. A. Shah, and P. A. Ganai, "Nanoporous anodic alumina (NAA) prepared in different electrolytes with different pore sizes for humidity sensing," *Journal of Solid State Electrochemistry*, vol. 24, no. 7, pp. 1679–1686, 2020, doi: 10.1007/s10008-020-04683-2.

[8] Y. F. Sun, S. B. Liu, F. L. Meng, J. Y. Liu, Z. Jin, L. T. Kong, J. H. Liu, "Metal oxide nanostructures and their gas sensing properties: a review", *Sensors (Basel),* vol. 12, no. 3, pp. 2610-2631, 2012, doi: 10.3390/s120302610.

[9] L. Manjakkal, K. Cvejin, J. Kulawik, K. Zaraska, R. P. Socha, and D. Szwagierczak, "X-ray photoelectron spectroscopic and electrochemical impedance spectroscopic analysis of RuO_2 -Ta_2O_5 thick film pH sensors," *Analytica Chimica Acta*, vol. 931, pp. 47–56, 2016, doi: 10.1016/j.aca.2016.05.012.

[10] C. H. Lin, S. J. Chang, and T. J. Hsueh, "Three-Dimensional ZnO Nanostructure Based Gas and Humidity Sensors," *Journal of Nanoscience and Nanotechnology*, vol. 18, no. 2, pp. 1202–1206, 2018, doi: 10.1166/jnn.2018.13976.

[11] H. Monreal et al., "Synthesis and characterization of Ta_2O_5 nanoparticles by sol-gel technique in a polysaccharide matrix," *Digest Journal of Nanomaterials and Biostructures*, vol. 11, no. 3, pp. 991–996, 2016.

[12] J. Ma, R. Zan, W. Chen, and J. Ni, "Cell behaviors on surface of pure tantalum with nano-dimpled structure," *Rare Metals*, vol. 38, no. 6, pp. 543–551, 2019, doi: 10.1007/s12598-019-01226-1.

[13] S. Zhang, S. Zhang, F. Peng, H. Zhang, H. Liu, and H. Zhao, "Electrodeposition of polyhedral Cu_2O on TiO_2 nanotube arrays for enhancing visible light photocatalytic performance," *Electrochemistry Communications*, vol. 13, no. 8, pp. 861–864, 2011, doi: 10.1016/j.elecom.2011.05.022.

[14] Y. Liu, C. Bao, D. Wismeijer, and G. Wu, "The physicochemical/biological properties of porous tantalum and the potential surface modification techniques to improve its clinical application in dental implantology," *Materials Science and Engineering: C*, vol. 49, no. 14, pp. 323–329, 2015, doi: 10.1016/j.msec.2015.01.007.

[15] W. J. Stepniowski and W. Z. Misiolek, "Review of fabrication methods, physical properties, and applications of nanostructured copper oxides formed via electrochemical oxidation," *Nanomaterials*, vol. 8, no. 6, pp. 1–19, 2018, doi: 10.3390/nano8060379.

[16] Z. Su, S. Grigorescu, L. Wang, K. Lee, and P. Schmuki, "Fast fabrication of Ta_2O_5 nanotube arrays and their conversion to Ta_3N_5 for efficient solar driven water splitting," *Electrochemistry Communications*, vol. 50, pp. 15-19, 2015, doi: 10.1016/j.elecom.2014.10.017.

[17] S. Xia, J. Ni, S. V Savilov, and L. Li, "Oxygen-deficient Ta_2O_5 nanoporous films as self-supported electrodes for lithium microbatteries," *Nano Energy*, vol. 45, pp. 407–412, 2018, doi: 10.1016/j.nanoen.2018.01.026.

[18] M. M. Momeni, "Effect of Composition Electrolyte on the Morphology and Photo Catalytic Activity of Anodized Titanium Nanoporous," *Journal*

of Nanostructures, vol. 9, no. 1, pp. 154–162, 2019, doi: 10.22052/JNS.2019.01.017.

[19] B. S. Vadlamani, T. Uppal, and S. C. Verma, "Functionalized TiO_2 Nanotube-Based Electrochemical Biosensor for Rapid Detection of SARS-CoV-2," *Sensors*, vol. 20, no. 20, pp. 5871, 2020.

[20] N. K. Awad, S. L. Edwards, and Y. S. Morsi, "A review of TiO_2 NTs on Ti metal: Electrochemical synthesis, functionalization and potential use as bone implants", *Materials Science & Engineering C*, vol. 1, no. 76, pp. 1401-1412, 2017, doi: 10.1016/j.msec.2017.02.150.

[21] M. M. M. M. Mirhosseini, M. Chavoshi, and A. Hakimizade, "The effect of anodizing voltage on morphology and photocatalytic activity of tantalum oxide nanostructure," *Journal of Materials Science: Materials in Electronics*, vol. 27, pp. 3941–3947, 2016, doi: 10.1007/s10854-015-4246-y.

[22] R. V Gonçalves et al., "Photochemical Hydrogen Production of TaO Nanotubes Decorated Photochemical Hydrogen Production of Ta_2O_5 Nanotubes Decorated with NiO Nanoparticles by Modified Sputtering Deposition," *Journal of Physical Chemistry A*, vol. 121, no. 11, pp. 5855–5863, 2017, doi: 10.1021/acs.jpcc.6b10540.

[23] M. M. Momeni, M. Mirhosseini, and M. Chavoshi, "Fabrication of Ta_2O_5 nanostructure films via electrochemical anodisation of tantalum," *Surface Engineering*, vol. 33, no. 2, pp. 83-89, 2016, doi: 10.1179/1743294415Y.0000000071.

[24] M. A. Baluk, M. P. Kobylański, W. Lisowski, G. Trykowski, T. Klimczuk, P. Mazierski, and A. Zaleska-Medynska, "Fabrication of Durable Ordered Ta_2O_5 Nanotube Arrays Decorated with Bi_2S_3 Quantum Dots," *Nanomaterials*, vol. 9, no. 10, pp. 1347, 2019, doi: 10.3390/nano9101347.

[25] M. A. Abu Talip et al., "Nanotubular Ta_2O_5 as ultraviolet (UV) photodetector," *Journal of Materials Science: Materials in Electronics*, vol. 30, no. 5, pp. 4953–4966, 2019, doi: 10.1007/s10854-019-00792-5.

[26] C. F. A. Alves, S. V Calderon, P. J. Ferreira, L. Marques, and S. Carvalho, "Passivation and dissolution mechanisms in ordered anodic tantalum oxide nanostructures," *Applied Surface Science*, vol. 513, pp. 145575, 2020, doi: 10.1016/j.apsusc.2020.145575.

[27] M. A. Abu Talip et al., "Mechanism of Nanotubular Ta_2O_5 via Anodization in NH 4 F / H 2 SO 4 / H 2 O Solution," *Journal of Electrical & Electronic Systems Research*, vol. 14, pp. 2–9, 2018. doi: 10.13140/RG.2.2.32329.47204

[28] J. D. Sloppy, Z. Lu, E. C. Dickey, and D. D. MacDonald, "Growth mechanism of anodic tantalum pentoxide formed in phosphoric acid," *Electrochimica Acta*, vol. 87, pp. 82–91, 2013, doi: 10.1016/j.electacta.2012.08.014.

[29] W. Wei, J. M. Macak, and P. Schmuki, "High aspect ratio ordered nanoporous Ta_2O_5 films by anodization of Ta," *Electrochemistry Communications*, vol. 10, pp. 428–432, 2008, doi: 10.1016/j.elecom.2008.01.004.

[30] K. Indira, S. Ningshen, U. K. Mudali, and N. Rajendran, "Effect of anodization parameters on the structural morphology of titanium in fluoride containing electrolytes," *Materials Characterization*, vol. 71, pp. 58–65, 2012, doi: 10.1016/j.matchar.2012.06.005.

[31] Agnieszka Brzózka, Anna Brudzisz, Dominika Rajska, Joanna Bogusz, Renata Palowska, Dominik Wójcikiewicz, Grzegorz D. Sulka., "Chapter two - Recent trends in synthesis of nanoporous anodic aluminum oxides," in *Nanostructured Anodic Metal Oxides*, Elsevier, 2020, pp. 35-88, doi: 10.1016/B978-0-12-816706-9.00002-9..

[32] M. Sarraf, B. A. Razak, B. Nasiri-Tabrizi, A. Dabbagh, N. H. A. Kasim, W. J. Basirun, E. Sulaiman, "Nanomechanical properties, wear resistance and in-vitro characterization of Ta_2O_5 nanotubes coating on biomedical grade Ti–6Al–4V", *Journal of the Mechanical Behavior of Biomedical Materials*, vol. 66, pp. 159-171, 2017, doi: 10.1016/j.jmbbm.2016.11.012.

[33] K. Lee and P. Schmuki, "Highly ordered nanoporous Ta_2O_5 formed by anodization of Ta at high temperatures in a glycerol/phosphate electrolyte," *Electrochemistry Communications*, vol. 13, pp. 542–545, 2011, doi: 10.1016/j.elecom.2011.03.005.

[34] W. Chen et al., "Study on morphology evolution of anodic tantalum oxide films in different using stages of H_2SO_4/HF electrolyte," *Electrochimica Acta*, vol. 236, pp. 140-153, 2017, doi: 10.1016/j.electacta.2017.03.024.

[35] P. Shang, S. Xiong, L. Li, D. Tian, and W. Ai, "Investigation on thermal stability of Ta_2O_5, TiO_2 and Al_2O_3 coatings for application at high temperature," *Applied Surface Science*, vol. 285, pp. 713–720, 2013, doi: 10.1016/j.apsusc.2013.08.115.

[36] I. Novianty, K. B. Seminar, Irzaman, and I. W. Budiastra, "Thin Film Electrical Photoconductivity of Ta_2O_5 Doped Based on Ba0.5S0.5TiO3 Thin Film," *IOP Conference Series: Earth and Environmental Science*, vol. 187, pp. 0–7, 2018.

[37] E. E. Nikishina, E. N. Lebedeva, and D. V Drobot, "Niobium- and tantalum-containing oxide materials: Synthesis, properties, and application," *Inorganic Materials*, vol. 48, no. 13, pp. 1243–1260, 2012, doi: 10.1134/s002016851213002x.

[38] S. Minagar, C. Berndt, and C. Wen, "Fabrication and Characterization of Nanoporous Niobia, and Nanotubular Tantala, Titania and Zirconia via Anodization," *Journal of Functional Biomaterials*, vol. 6, no. 2, pp. 153–170, 2015, doi: 10.3390/jfb6020153.

[39] P. Migowski et al., "Ta_2O_5 Nanotubes Obtained by Anodization: Effect of Thermal Treatment on the Photocatalytic Activity for Hydrogen

Production," *The Journal of Physical Chemistry C*, vol. 116, no. 26, pp. 14022–14030, 2012.

[40] E. Uslu, H. Öztatl, B. Garipcan, and B. Ercan, "Fabrication and cellular interactions of nanoporous tantalum oxide," *Journal of Biomedical Materials Research Part B: Applied Biomaterials*, vol. 108, no. 7 pp. 2743-2753, 2020, doi: 10.1002/jbm.b.34604.

[41] J. Ni and M. Sun, "Chapter nine - Anodic tantalum oxide: synthesis and energy-related applications," in *Nanostructured Anodic Metal Oxides*, pp. 305–320, 2020, doi: 10.1016/B978-0-12-816706-9.00009-1

[42] L. Fialho, C. F. A. Alves, L. S. Marques, and S. Carvalho, "Development of stacked porous tantalum oxide layers by anodization," *Applied Surface Science*, vol. 511, no. 1, pp. 145542, 2020, doi: 10.1016/j.apsusc.2020.145542.

[43] G. Chen, A.-C. Cho, S.-T. Chen, and Y.-C. Chen, "Electrochemical Anodization of 2-nm-Thick Tantalum Films for Self- Assembling of Molecularly Thick Layer as a Barrier for Copper*," Journal of The Electrochemical Society*, vol. 167, no. 11, pp. 112506, 2020, doi:10.1149/1945-7111/aba15d

[44] N. Alias, S. A. Rosli, N. Bashirom, M. Rozana, W. K. Tan, G. Kawamura, P. Nbelayim, A. Matsuda, Z. Hussain, Z. Lockman, "Chapter eight - Oxide nanotubes formation by anodic process and their application in photochemical reactions for heavy metal removal," in *Nanostructured Anodic Metal Oxides*, pp. 277–304, 2020, doi: 10.1016/B978-0-12-816706-9.00008-X.

[45] M. Sarraf, B. Nasiri-Tabrizi, C. H. Yeong, H. R. M. Hosseini, S. Saber-Samandari, W. J. Basirun, T. Tsuzuki, "Mixed oxide nanotubes in nanomedicine: A dead-end or a bridge to the future?," *Ceramics International*, vol. 47, no. 3, pp. 2917-2948, 2021, doi: 10.1016/j.ceramint.2020.09.177.

[46] R. Kant, R. Tabassum, and B. D. Gupta, "Xanthine oxidase functionalized Ta_2O_5 nanostructures as a novel scaffold for highly sensitive SPR based fiber optic xanthine sensor," *Biosensors and Bioelectronics*, vol. 99, pp. 637-645, 2018, doi: 10.1016/j.bios.2017.08.040.

[47] Z. Zhang, Z. Wen, Z. Ye, and L. Zhu, "Synthesis of Co_3O_4/ Ta_2O_5 heterostructure hollow nanospheres for enhanced room temperature ethanol gas sensor," *Journal of Alloys and Compounds*, vol. 727, pp. 436-443, 2017, doi: 10.1016/j.jallcom.2017.07.181.

[48] H. Yu, S. Zhu, X. Yang, X. Wang, H. Sun, and M. Huo, "Synthesis of Coral-Like Tantalum Oxide Films via Anodization in Mixed Organic-Inorganic Electrolytes," *PLoS One*, vol. 8, no. 6, pp. 6–11, 2013, doi: 10.1371/journal.pone.0066447.

[49] T. Wen et al., "Growth behavior of tantalum oxide nanotubes during constant current anodization," *Electrochemistry Communications*, vol. 128, pp. 107073, 2021, doi: 10.1016/j.elecom.2021.107073.

[50] N. Mohammadian, S. Faraji, S. Sagar, and B. C. Das, "One-Volt, Solution-Processed Organic Transistors with Self-Assembled Monolayer-Ta_2O_5 Gate Dielectrics," *Materials*, vol. 12, pp. 2563, 2019.

[51] R. Nakamura, K. Asano, M. Ishimaru, K. Sato, M. Takahashi, and H. Numakura, "Stability of amorphous Ta-O nanotubes prepared by anodization: Thermal and structural analyses," *Journal of Materials Research*, vol. 29, no. 6, pp. 753–760, 2014, doi: 10.1557/jmr.2014.44.

[52] R. A. Rani, S. Zoolfakar, A. P. O. Mullane, M. W. Austin, and K. Kalantar-zadeh, "Thin films and nanostructures of niobium pentoxide : fundamental properties, synthesis methods and applications," *Journal of Materials Chemistry A*, vol. 2, pp. 15683–15703, 2014, doi: 10.1039/C4TA02561J.

[53] M. Sowa et al., "Influence of process parameters on plasma electrolytic surface treatment of tantalum for biomedical applications," *Applied Surface Science*, vol. 407, pp. 52–63, 2017, doi: 10.1016/j.apsusc.2017.02.170.

[54] Y. Hong et al., "A visible-light-driven heterojunction for enhanced photocatalytic water splitting over Ta_2O_5 modified g-C_3N_4 photocatalyst," *International Journal of Hydrogen Energy*, vol. 42, no. 10, pp. 6738–6745, 2017, doi: 10.1016/j.ijhydene.2016.12.055.

[55] L. Fialho and S. Carvalho, "Surface engineering of nanostructured Ta surface with incorporation of osteoconductive elements by anodization," *Applied Surface Science*, vol. 495, pp. 143573, 2019, doi: 10.1016/j.apsusc.2019.143573.

[56] R. Kisslinger et al., "Nonlithographic Formation of Ta_2O_5 Nanodimple Arrays Using Electrochemical Anodization and Their Use in Plasmonic Photocatalysis for Enhancement of Local Field and Catalytic Activity," *ACS Applied Materials & Interfaces*, vol. 13, no. 3, 2021, doi: 10.1021/acsami.0c18580.

[57] P. Chakraborti, H. Sharma, and M. Raj, "Oxide composition studies of electrochemically grown tantalum oxide on sintered tantalum using XPS depth-profiling and co- relation with leakage properties", *Journal of Materials Science: Materials in Electronics*, vol. 28, pp. 18773–18780, 2017, doi: 10.1007/s10854-017-7826-1.

[58] Y. Li, K. Nagato, J. Delaunay, et al, "Fabrication of highly ordered Ta_2O_5 and Ta_3N_5 nanorod arrays by nanoimprinting and through-mask anodization," *Nanotechnology*, vol. 25, 2014, doi: 10.1088/0957-4484/25/1/014013.

[59] X. Lü et al., "Pressure-induced amorphization in single-crystal Ta_2O_5 nanowires: A kinetic mechanism and improved electrical conductivity," *Journal of the American Chemical Society*, vol. 135, no. 37, pp. 13947–13953, 2013, doi: 10.1021/ja407108u.

[60] G. Nagaraju, K. Karthik, and M. Shashank, "Ultrasound-assisted Ta_2O_5 nanoparticles and their photocatalytic and biological applications,"

Microchemical Journal, vol. 147, pp. 749–754, 2019, doi: 10.1016/j.microc.2019.03.094.

[61] Adel A. Ismail, M. Faisal, Farid A. Harraz, A. Al-Hajry, A.G. Al-Sehemi, "Synthesis of Mesoporous Sulfur-Doped Ta_2O_5 Nanocomposites and Their Photocatalytic Activities," *Journal of Colloid and Interface Science*, vol. 471, pp. 145-154, 2016, doi: 10.1016/j.jcis.2016.03.019.

[62] M. K. Patil, H. C. Bajaj, and R. J. Tayade, "Synthesis and characterization of tantalum based photocatalysts and application for methylene blue degradation," *Materials Science Forum*, vol. 855, pp. 147–155, 2016, doi: 10.4028/www.scientific.net/MSF.855.147.

[63] S. Maeng, L. Axe, T. Tyson, and A. Jiang, "An Investigation of Structures of Thermal and Anodic Tantalum Oxide Films," *Journal of The Electrochemical Society*, vol. 152, no.2, pp. 3–8, 2005, doi: 10.1149/1.1850362.

[64] R. S. Brown, "Investigating the properties and application of tantalum pentoxide nanostructures for cancer radiotherapy", University of Wollongong, Wollongong, 2017.

[65] A. Cacucci, S. Loffredo, V. Potin, L. Imhoff, and N. Martin, "Interdependence of structural and electrical properties in tantalum/tantalum oxide multilayers," *Surface and Coatings Technology*, vol. 227, pp. 38–41, 2013, doi: 10.1016/j.surfcoat.2012.10.064.

[66] D. J. Werder and R. R. Kola, "Microstructure of Ta_2O_5 films grown by the anodization of TaNx," *Thin Solid Films*, vol. 323, pp. 6–9, 1998.

[67] G. Mohandas, N. Oskolkov, M. T. McMahon, P. Walczak, and M. Janowski, "Porous tantalum and tantalum oxide nanoparticles for regenerative medicine," *Acta Neurobiologiae Experimentalis*, vol. 74, no. 2, pp. 188–196, 2014.

[68] V. K. Balla, S. Bodhak, S. Bose, and A. Bandyopadhyay, "Porous tantalum structures for bone implants: Fabrication, mechanical and in vitro biological properties," *Acta Biomaterialia*, vol. 6, no. 8, pp. 3349–3359, 2010, doi: 10.1016/j.actbio.2010.01.046.

[69] M. S. Farhan, E. Zalnezhad, and A. R. Bushroa, "Properties of Ta_2O_5 thin films prepared by ion-assisted deposition," *Materials Research Bulletin*, vol. 48, pp. 4206–4209, 2013, doi: 10.1016/j.materresbull.2013.06.068.

[70] Luiz E. Gomes et al., "Synthesis and Visible-Light-Driven Photocatalytic Activity of Ta^{4+} Self-Doped Gray Ta_2O_5 Nanoparticles," *The Journal of Physical Chemistry C*, vol. 122, no. 11, 6014–6025, 2018, doi: 10.1021/acs.jpcc.7b11822.

[71] R. Kant and R. Tabassum, "Mechanistic Modeling for Performance Engineering of SPR-Based Fiber-Optic Sensor Employing Ta_2O_5 and Graphene Multilayers in Phase Interrogation Scheme," *Plasmonics*, vol 15, pp. 647–659, 2020, doi: 10.1007/s11468-019-01065-x

[72] V. A. Online, R. Nashed, W. M. I. Hassan, Y. Ismail, and N. K. Allam, "Unravelling the interplay of crystal structure and electronic band

structure of tantalum oxide (Ta_2O_5)," *Physical chemistry chemical physics: PCCP*, vol. 15, no. 5, pp. 1352–1357, 2013, doi: 10.1039/c2cp43492j.

[73] B. Niu, Z. Chen, and Z. Xu, "Recycling waste tantalum capacitors to synthesize high value-added Ta_2O_5 and polyaniline-decorated Ta_2O_5 photocatalyst by an integrated chlorination-sintering-chemisorption process," *Journal of Cleaner Production*, vol. 252, pp. 117206, 2020, doi: 10.1016/j.jclepro.2019.06.037.

[74] H. Krysova, P. Mazzolini, C. S. Casari, V. Russo, A. L. Bassi, and L. Kavan, "Electrochemical Properties of Transparent Conducting Films of Tantalum-Doped Titanium Dioxide," *Electrochimica Acta*, vol. 232, pp. 44–53, 2017, doi: 10.1016/j.electacta.2017.02.124.

[75] M. R. Nickel, G. Melligan, T. P. W. Mcmullen, and R. E. Burrell, "The effect of chemical additives in phosphoric acid anodization of aluminum-tantalum thin films," *Thin Solid Films*, vol. 685, pp. 245–253, 2019, doi: 10.1016/j.tsf.2019.06.033.

[76] M. Al-hashem, S. Akbar, and P. Morris, "Role of Oxygen Vacancies in Nanostructured Metal-Oxide Gas Sensors : A Review," *Sensors and Actuators B: Chemical*, vol. 301, pp. 126845, 2019, doi: 10.1016/j.snb.2019.126845.

[77] L. J. Bannenberg, C. Boelsma, H. Schreuders, S. Francke, N. J. Steinke, and A. A. Van Well, "Optical hydrogen sensing beyond palladium : Hafnium and tantalum as effective sensing materials," *Sensors and Actuators. B, Chemical*, vol. 283, pp. 538–548, 2019, doi: 10.1016/j.snb.2018.12.029.

[78] A. Imbault et al., "Ultrathin Gas Permeable Oxide Membranes for Chemical Sensing : Nanoporous Ta_2O_5 Test Study," *Materials*, vol. 8, pp. 6677–6684, 2015, doi: 10.3390/ma8105333.

[79] L. Manjakkal, K. Zaraska, J. Kulawik, and D. Szwagierczak, "Potentiometric RuO_2- Ta_2O_5 pH Sensors fabricated using thick film and LTCC Technologies," *Talanta*, vol. 147, pp. 233-240, 2016, doi: 10.1016/j.talanta.2015.09.069.

[80] M. Chen, Y. Jin, X. Qu, Q. Jin, and J. Zhao, "Electrochemical impedance spectroscopy study of Ta_2O_5 based EIOS pH sensors in acid environment," *Sensors and actuators. B, Chemical*, vol. 192, pp. 399–405, 2014, doi: 10.1016/j.snb.2013.10.129.

[81] L. M. Kuo, Y. C. Chou, K. N. Chen, C. C. Lu, and S. Chao, "A precise pH microsensor using RF-sputtering IrO_2 and Ta_2O_5 films on Pt-electrode," *Sensors and Actuators. B, Chemical*, vol. 193, pp. 687–691, 2014, doi: 10.1016/j.snb.2013.11.109.

[82] L. Manjakkal, K. Cvejin, B. Bajac, J. Kulawik, K. Zaraska, and D. Szwagierczak, "Microstructural, Impedance Spectroscopic and Potentiometric Analysis of Ta_2O_5 Electrochemical Thick Film pH

Sensors," *Electroanalysis*, vol. 27, no. 3, pp. 770–781, 2015, doi: 10.1002/elan.201400571.

[83] R. Zhao, M. Xu, J. Wang, and G. Chen, "A pH sensor based on the TiO_2 nanotube array modified Ti electrode," *Electrochimica Acta*, vol. 55, no. 20, pp. 5647–5651, 2010, doi: 10.1016/j.electacta.2010.04.102.

[84] E. Nycander, "Evaluation of ALD Oxides as the Sensing Layer for Ion Sensors," Uppsala Universitet, 2016.

[85] A. Prak, H. H. Van Den Vlekkert, and M. Levine, "Ultraminiature ph isfet with back side contacts and Ta_2O_5 gate material for use in a guidewire tip," in *The 3rd Conference on MicroFluidic Handling Systems*, Sensors, vol. 11, no. 5, pp. 4562-4571.

[86] S. Singh, G. Gupta, S. Yadav, and P. K. Dubey, Highly-sensitive potassium-tantalum-niobium oxide humidity sensor," *Sensors and actuators. A, Physical*, vol. 295, pp. 133–140, 2019, doi: 10.1016/j.sna.2019.05.023.

[87] J. J. Steele, M. T. Taschuk, M. J. Brett, and I. Terms, "Nanostructured Metal Oxide Thin Films for Humidity Sensors," *IEEE Sensors Journal*, vol. 8, no. 8, pp. 1422–1429, 2008.

[88] D. Nunes et al., "Metal oxide nanostructures for sensor applications," *Semiconductor Science and Technology*, vol. 34, no. 4, pp. 043001, 2019, doi: 10.1088/1361-6641/ab011e

[89] Y. Zhang, K. Yu, D. Jiang, Z. Zhu, H. Geng, and L. Luo, "Zinc oxide nanorod and nanowire for humidity sensor," *Applied Surface Science*, vol. 242, no. 1-2, pp. 212–217, 2005, doi: 10.1016/j.apsusc.2004.08.013.

[90] H. Farahani, R. Wagiran, and M. N. Hamidon, "Humidity Sensors Principle, Mechanism, and Fabrication Technologies: A Comprehensive Review," *Sensors*, vol. 14, pp. 7881–7939, 2014, doi: 10.3390/s140507881.

[91] B. Chethan, H. G. R. Prakash, Y. T. Ravikiran, S. C. Vijayakumari, and S. Thomas, "Polypyyrole based core-shell structured composite based humidity Sensor operable at room temperature," *Sensors and Actuators. B, Chemical*, vol. 296, pp. 126639, 2019, doi: 10.1016/j.snb.2019.126639.

[92] S. Karthick, H. Lee, S. Kwon, and R. Natarajan, "Standardization, Calibration, and Evaluation of Tantalum-Nano rGO-SnO_2 Composite as a Possible Candidate Material in Humidity Sensors," *Sensors*, vol. 16, no. 12, pp. 2079, 2016, doi: 10.3390/s16122079.

[93] C. K. Chung, O. K. Khor, E. H. Kuo, and C. A. Ku, "Total effective surface area principle for enhancement of capacitive humidity sensor of thick-film nanoporous alumina," *Materials Letters*, vol. 260, pp. 126921, 2020, doi: 10.1016/j.matlet.2019.126921.

[94] A. Pawlik, K. Hnida, R. P. Socha, E. Wiercigroch, K. Małek, and G. D. Sulka, "Effects of anodizing conditions and annealing temperature on the morphology and crystalline structure of anodic oxide layers grown on

iron," *Applied Surface Science*, vol. 426, pp. 1084–1093, 2017, doi: 10.1016/j.apsusc.2017.07.156.

[95] R. S. Khaleel and M. S. Hashim, "Fabrication of ZnO sensor to measure pressure , humidity and sense vapors at room temperature using the rapid breakdown anodization method," *Kuwait Journal of Science*, vol. 47, no. 1, pp. 42–49, 2020.

[96] Y. He and Y. Yang, "Helical Mesoporous Tantalum Oxide Nanotubes : Formation , Optical Activity , and Applications," *The Chemical Record*, vol. 17, no. 11, pp. 1146-1155, 2017, doi: 10.1002/tcr.201700012.

[97] V. Khanal, R. Irani, S. Fiechter, F. F. Abdi, and V. (Ravi) Subramanian, "The Photoelectrochemical and Photocatalytic Properties of Tantalum Oxide and Tantalum Nitride," *Journal of The Electrochemical Society*. vol. 166, no. 5, pp. 3294–3299, 2019, doi: 10.1149/2.0391905jes.

[98] N. L. S. Ngadiman, R. Abdul Rani, Z. F. Zulkifli, M. F. Abdullah, S. R. Makhsin, M. Zolkapli, A. S. Zoolfakar, and M. Nour, "Preliminary Study of pH Sensor for Engine Oil Deterioration Detection Using Anodized Ta_2O_5 Nanotubular," *International Journal of Integrated Engineering*, vol. 14, no.3, pp. 229–240, 2022, doi: 10.30880/ijie.2022.14.03.025

[99] N.L.S. Ngadiman, R. Abdul Rani, S. R. Makhsin, et al. "Facile fabrication method and decent humidity sensing of anodised nanotubular Ta_2O_5 on Ta foil substrate," *Journal of Materials Science: Materials in Electronics*, vol. 33, pp. 3065–3080, 2022, doi: 10.1007/s10854-021-07509-7